UiT THE ARCTIC UNIVERSITY OF NORWAY

Faculty of Science and Technology

Department of Geosciences

Paleoceanographic Development in Nordfjord, North East Greenland, During the Mid- and Late Holocene

Bjørnar Liland Skjelvan

GEO-3900 Master's thesis in Geology

May 2017

Abstract

Sediment core HH13-012GC-TUNU, retrieved from Nordfjord, North-East Greenland, has been investigated in order to reconstruct the paleoceanographic development during the mid- and late Holocene. Nordfjord is one of three tributary fjords to Kaiser Franz Joseph Fjord, and Waltershausen Gletcher is located at its head. The fjord system is largely influenced by the Eastern Greenland Current.

Most of the paleoceanographic research from fjords in Greenland have been done in the south-east, and south-west, whereas there are very few studies from the north-eastern part. In this study, results from the sediment core HH13-012GC-TUNU are based on benthic foraminiferal assemblages. An age model is established based on two AMS ^{14}C dates, in addition to an assumed age of the uppermost part. From the results, three foraminiferal assemblage zones are established within the last ~7800 cal. yr. BP, covering the Holocene Climate Optimum, the Neoglaciation, and the Little Ice Age. The strong dominance of the species *Cassidulina reniforme* throughout the core indicates that the conditions within Nordfjord have been that of a glaciomarine environment during the last ~7800 cal. yr. High relative abundance of *Islandiella Helenae* indicates that Atlantic Water, and seasonal sea ice conditions influenced the area until ~5200 cal. yr. BP. The transition from the Holocene Climate Optimum to the Neoglaciation is marked by an abrupt increase in the cold water species *Astrononion Gallowayi*, indicating inflow of Arctic Water, combined with higher energy conditions. The last ~630 cal. yr. BP is dominated by *Elphidium excavatum* f. *clavata*, indicating continued inflow of Arctic Water, combined with seasonal sea ice cover.

Forord

Først og fremst vil jeg takke mine to dyktige veiledere, Katrine Husum og Jan Sverre Laberg. Takk for at dere alltid har vert tilgjengelig med god veiledning, kritisk gjennomlesing og tilbakemeldinger underveis i prosessen. I tillegg er jeg takknemlig for at dere gjorde det mulig for meg å delta på tokt med Norsk Polarinstitutt. Dette var svært lærerikt, og gav meg et innblikk i hvordan livet til en geolog kan være.

Takk til Karina Monsen og Trine Dahl for all hjelp på laboratoriet. Samt en takk til ansatte ved UiT, og medstudenter som var behjelpelige med identifisering av arter.

Jeg vil også takke alle medstudenter som jeg har blitt kjent med gjennom mine 5 år ved UiB og UiT, som jeg har delt mange minneverdige opplevelser med. En ekstra takk sendes til Jarl-Eirik, June, Jørn og Petter for lange kaffepauser og nødvendige distraksjoner i en heller hektisk hverdag det siste året.

Til slutt vil jeg rette en stor takk til mine foreldre, og resten av familien. Tusen takk for oppmuntring, gode råd, språkvask, og ikke minst finansiell støtte gjennom alle årene som student. Jeg er evig takknemlig.

Bjørnar Liland Skjelvan

Tromsø, 15. mai 2017

List of content

1. Introduction

1.1 Objectives

The primary objective of this study is to reconstruct the paleoceanography and paleoclimate in Nordfjord in the northeast of Greenland during the Holocene. By looking at benthic foraminiferal records from sediment core HH13-012GC-TUNU, changes in water masses and seafloor environment should be identified.

1.2 Paleoceanography and paleoclimate

Paleoceanography is the scientific study of changes in the oceans' characteristics regarding e.g. chemistry, circulation and temperature over time, whereas paleoclimate is the study of past climates during time. Ocean currents are driven by differences in density, where temperature and salinity plays a major role. Changes in these parameters can slow down, or increase the flow rate of ocean currents, and thereby influence the climate in certain regions. Reconstruction of paleoceanography and paleoclimate is done by analysing proxy data. Proxies are indirect measurements of past climate or environmental changes, and are found within e.g. ice cores and sediment cores. By considering the uniformitarian principle, "The present is the key to the past", samples found within ice cores or sediment cores can be compared to present day's environment. In this study, benthic foraminifera are analysed. As benthic foraminifera can be quite particular about which environment they thrive in, one can by applying transfer functions, correlate the foraminiferal assemblages found at different depths within a sediment core to specific bottom water temperatures (BWT) and bottom water salinity (BWS).

1.3 Evolution of paleoceanography and paleoclimate on East Greenland

1.3.1 Holocene paleoceanographic development

The circulation of surface water within the ocean, is mainly driven by atmospheric circulation. The circulation of deeper water masses is on the other hand, driven by differences in density, which come as a result of variations in temperature and salinity. This phenomena is called the thermohaline circulation (THC) (Bradley, 2015). The Greenland Sea is important to the global ocean circulation, as deep water convection occurs in this area. This again leads to the formation of North Atlantic Deep Water (NADW) (Marshall and Schott, 1999; Telesiński et al., 2014a). NADW forms as surface water cools, and increases in salinity north of ~ 60ºN, resulting in a dense water mass to sink and move southwards towards the South Atlantic. As a response to the formation of NADW, warm and saline surface waters move poleward within the Gulf Stream and North Atlantic Current. This process is termed the Atlantic Meridional Overturning Circulation (AMOC) (Bradley, 2015). The NADW circulation is severely sensitive to changes in salinity, and the entire process could wind down when the catchment area of the North Atlantic is added as little as 0,06 Sv (1 sverdrup = 10^6 m^3 s^{-1}) additional freshwater (Rahmstorf, 1995).

The two major surface-water masses influencing the area are the cold and low saline Polar Water (PW) transported southwards by the Eastern Greenland Current (EGC), and the relatively warm and saline Atlantic Water (AW) transported northwards by the North Atlantic Current (NAC) (Telesiński et al., 2014a) (Figure 1). During the Holocene, the paleoceanographic evolution of the Greenland Sea was primarily controlled by insolation, whereas variations in inflow of warm AW controlled the spatial variability (e.g. Telesiński et al., 2014b). During the early Holocene (11.9-7 ka) the surface water warmed up, which again led to an increase in productivity and the surface water ventilation improved. From 7-3 ka, during the Middle Holocene, there was a decrease in insolation, which led to the Neoglacial cooling that was enhanced by inflow to the area of cold PW. As a consequence of the Neoglacial cooling, at 3 ka the surface layer thickened, which rapidly decreased the ventilation and the stratification of the upper water mass became stronger. At ~2 ka the late Holocene warming occurred. This was caused by increased inflow of AW into the Nordic Seas (Telesiński et al., 2014a).

According to Jennings and Weiner (1996), there have during the last millennium been changes in both water masses and sea ice condition within the EGC. Their study is based on benthic and planktic foraminifera, lithofacies, and sedimentological analysis of two marine sediment cores collected from Nansen Fjord. Nansen Fjord is located in the south-eastern part of Greenland, and is thereby influenced by the EGC. The Medieval Warm Period (~730 AD – ~1110 AD) was a period which was characterized by a relatively warm and stable climate, and in Nansen Fjord this warming period was represented by Atlantic Intermediate Water dominating the fjord, either caused by relatively low influx of PW, or a strong influx of AW. Findings from diatom analysis from Kangerlussuaq Trough on the SE Greenland shelf, show that from ~1000 C.E, an abrupt warming occurred, increasing the sea surface temperature with ~2.4°C in only ~55 years (Miettinen et al., 2015).

The Little Ice Age followed the Medieval Warm Period, and in Nansen Fjord, South-Eastern Greenland, the conditions varied severely, with some brief periods with perennial sea-ice cover, indicating exceptionally cold conditions (Jennings and Weiner, 1996). Miettinen et al., (2015) suggest the same variations during the period, with cooling of the sea surface temperature from 1200-1600 CE, followed by a relatively warm period until 1820 CE, before reaching the coldest period within the last millennium, lasting until ~1890 CE.

Several studies propose that the positive phase of the Arctic Oscillation (AO)/North Atlantic Oscillation (NAO) was an important factor for the changes occurring during the MWP (e.g. Mann et al., 2009). The positive phase is associated with increased southwards sea ice export within the EGC from Fram Strait (Andrews and Jennings, 2014). Findings from the SE Greenland shelf indicate that both the MWP, and the transition to the LIA most likely were caused by a combination of solar- and atmospheric forcing (Miettinen et al., 2015). In their study, the authors claim that the Oort solar minimum could have triggered a rapid warming in the area. The Oort minimum could have led to a low melting rate of the Greenland Ice Sheet, again leading to a decreased sea ice formation. In addition, the authors found that NAO reached a high positive phase at the end of a high sea surface temperature event, and thereby possibly being the reason for the following cooling of the surface waters. According to Shindell et al., (2003), a combination of volcanic- and solar forcing was responsible for the global LIA signal. They claim that volcanic forcing played a major role of the global cooling during the LIA, whereas solar forcing was behind regional variations.

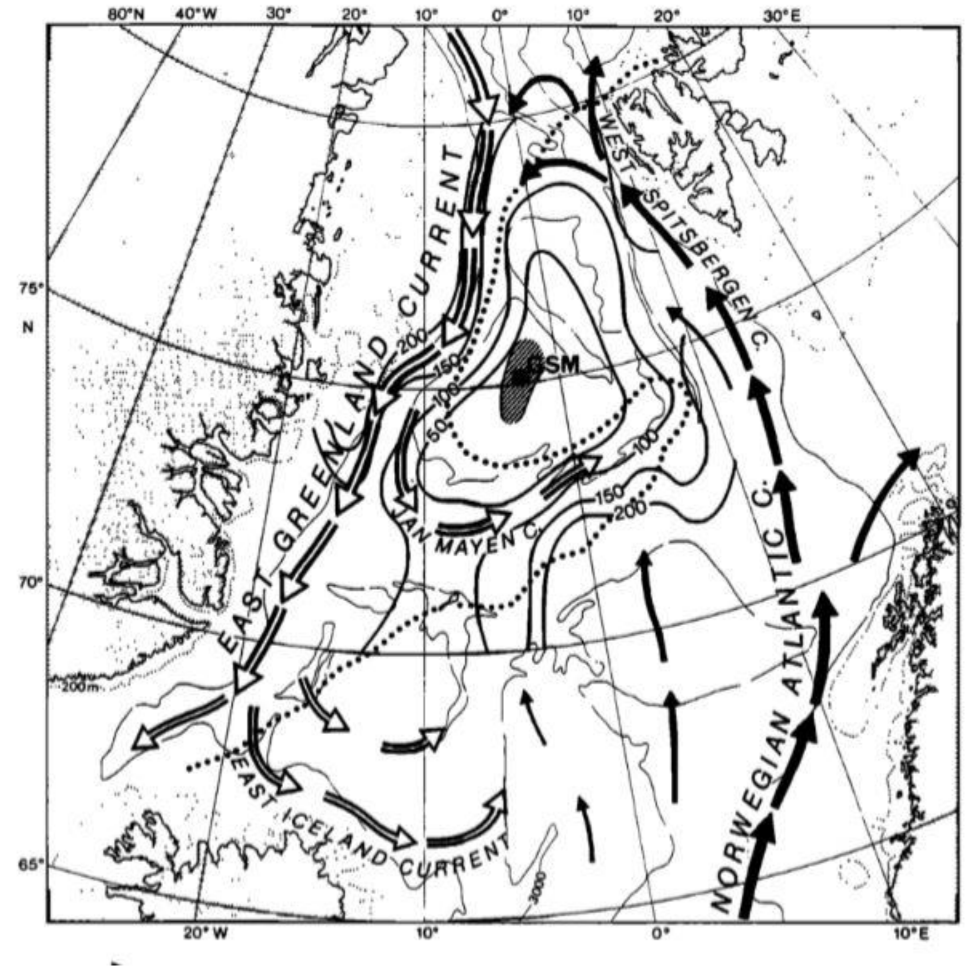

Figure 1: Overview of the main ocean currents affecting the Greenland Sea at present time. Black arrows indicate warm and saline Atlantic Water, whereas white arrows indicate cold and less saline Polar Water (Adapted from Marshall and Schott, 1999)

1.3.2 Holocene paleoclimate development

The climate in East Greenland is largely influenced by oceanic circulation and radiation energy. The further north, the cooler it is. This is related to the northward decrease in radiation energy, and northward increase in the influence of the cold EGC.

According to Wagner et al., (2000) records of climatic variations on East Greenland during the Holocene can be found from lake sediments formed after 9000 cal. yr. BP. During the early Holocene (9000 - 6500 cal. yr. BP) the climate consisted of warm summers and higher temperatures than at present, combined with high summer insolation. This period is called the early Holocene climatic optimum. Within the Holocene Climatic Optimum evidence has been found for a short lived cold event, lasting from 8300 – 8200 cal. yr. BP. This event is named the “8.2 ka event”, and was related to decrease in the salinity at the sea surface, and the strength of North Atlantic overturning circulation as a response to substantial outflow of freshwater from the Hudson Strait (Barber et al., 1999). This again led to an expansion of sea ice during winter time (Alley et al., 2010).

Following the early Holocene climatic optimum came a period with high precipitation rates, lasting until 3000 cal. yr. BP. The temperatures started decreasing at 5000 cal. yr. BP and lasted until approximately 1000 cal. yr. BP, making up a cold and dry climate the last 2000 years of the period (Wagner et al., 2000). The Neoglaciation started at least at 5000 cal. yr. BP, and led to glaciers expanding all over Greenland (Bennike and Weidick, 2001).

During the end of the Neoglaciation the Medieval Warm Period (MWP) occurred, associated with increasing temperatures. It lasted for approximately 200 years, before the Little Ice Age (LIA) commenced. The Little Ice Age lasted from about 800 to 100 cal. yr. BP, and was the coldest period within the Holocene. During the beginning of this period, the precipitation rates slightly increased (Wagner et al., 2000).

Following the LIA the temperatures started increasing again, followed by a cooling from the 1970s to early 1990s, and a new warming, finally reaching the present day temperatures (Kobashi et al., 2015).

1.4 Study Area

Greenland is the world’s largest island, and it is surrounded by the Arctic Ocean to the north, the Greenland Sea to the east, the Atlantic Ocean to the south, and Baffin Bay to the west. Overall Greenland has a total coastline of 44,087 km (Olsen, 2015), and approximately 80% of the overall area is covered by glaciers. As fjords are formed by land-based ice, the severe glaciological action that has been characterizing Greenland over time has formed fjords around almost the entire coastline, varying in range from a few kilometres up to hundreds of kilometres in length (Cottier et al., 2010).

The sediment core investigated in this study (HH13-012GC-TUNU) was collected from Nordfjord, one of the three main tributary fjords of Kaiser Franz Joseph Fjord, in the northeast of Greenland

(Figure 2). The other two tributary fjords making up the fjord system are Geologfjord and Isfjord. Overall the fjord system covers 2200 km^2, and stretches for 220 km from head to mouth (Evans et al., 2002). Both Kaiser Franz Joseph Fjord, and its related tributary fjords have glaciers terminating at their head. These glaciers are the results of The Greenland Ice Sheet draining through the inner coastal mountain zone. At the head of Nordfjord, Waltershausen Gletscher is terminating. This is the largest of the glaciers found within the Kaiser Franz Joseph Fjord system, and the width of the terminus is approximately 10.2 km (Evans et al., 2002).

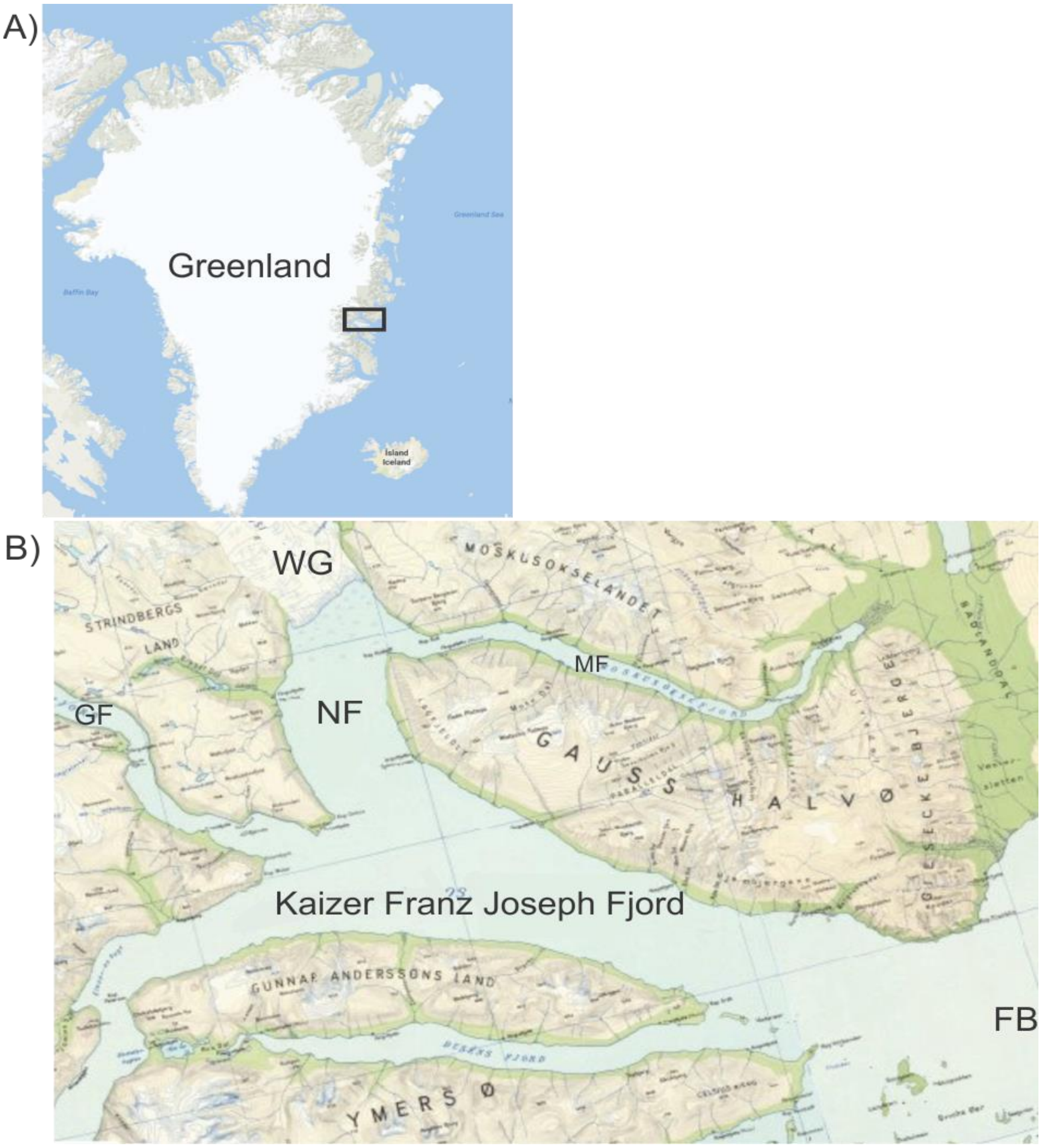

Figure 2A) Overview map of Greenland. The location of Kaiser Franz Joseph Fjord is indicated by a black square. Figure 2B shows Kaiser Franz Joseph Fjord, and its related tributary fjords and topography. NF-Nordfjord, GF - Geologfjord, MF - Moskusoksefjord, WG – Waltershausen Gletscher, FB – Fosters Bugt.

2. Physical and Geological Setting

2.1 Fjords

Syvitski et al., (1987) define a fjord as “a deep, high-latitude estuary which has been (or is presently being) excavated or modified by land-based ice”. The authors also describe fjords as transition zones between land and open ocean where there is a mixing of salt- and freshwater, with a resulting production of strong physical and chemical gradients.

Hambrey (1994) made a classification of fjords related to their glacial influence at present day conditions. His classification contains four regimes, Alaskan regime, Svalbard regime, Greenland regime, and Antarctic maritime regime. Kaiser Franz Joseph Fjord falls under the Greenland regime, which is characterized by dynamic, floating, cold glaciers in deep fjords, typically derived from the Greenland ice sheet.

Syvitski et al., (1987) divided the Greenland fjords into four quadrants, with Kaiser Franz Joseph Fjord located on the north-eastern coast (Figure 3). What characterizes the fjords in this zone is that they are cut in crystalline bedrock, and the fjords with a north-south trend are controlled by major fault zones.

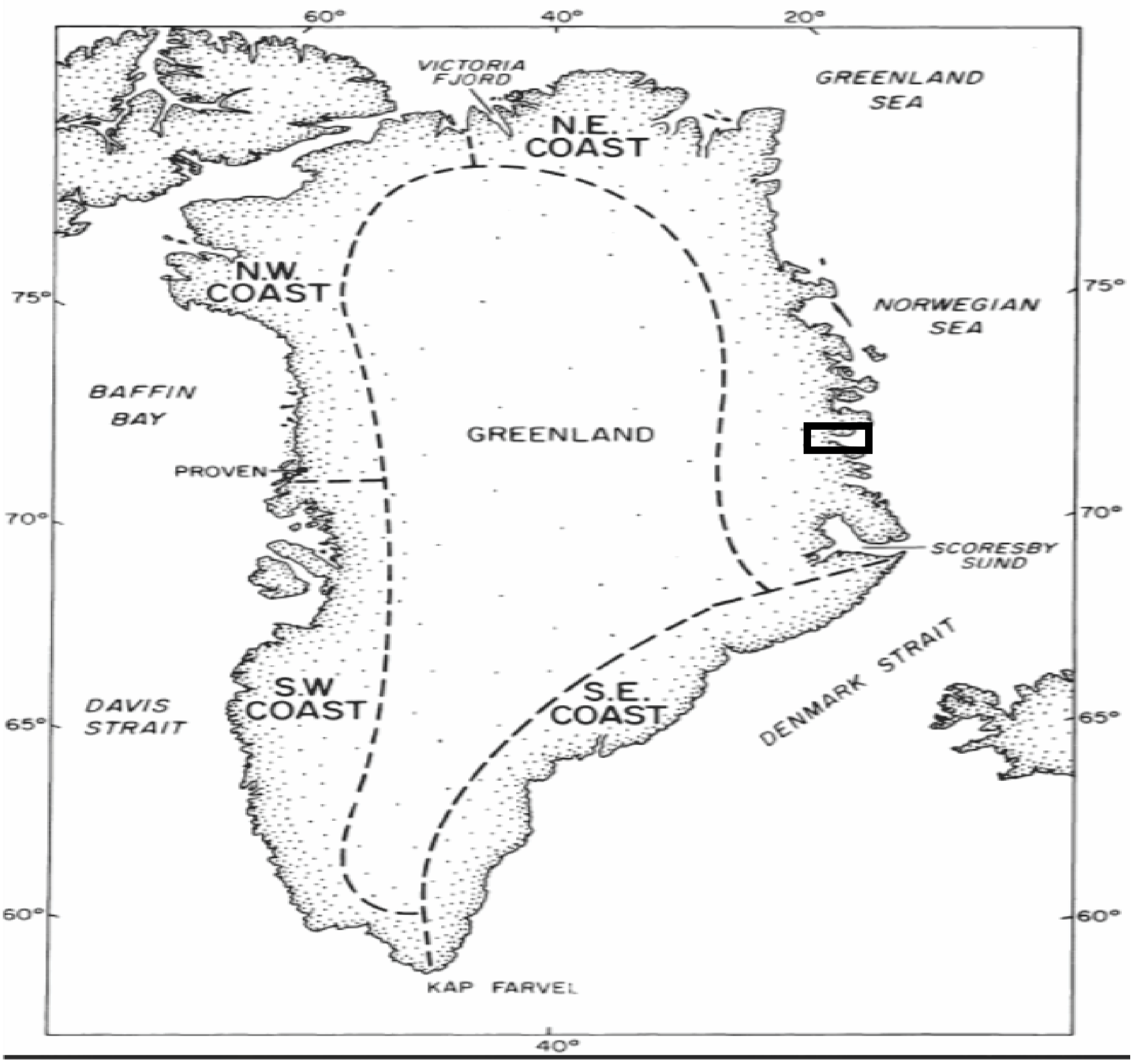

Figure 3: Greenland's four different fjord zones. The black square within the N.E. Coast zone indicates location of Kaiser Franz Joseph Fjord. Modified from Syvitski et al., (1987).

2.2 Bathymetry

According to Olsen, (2015), Nordfjord is approximately 35 km long, and 13 km wide, which makes it a relatively short and wide fjord. It follows a N-S trend, with Waltershausen Gletscher located at its head in the north. From the head of the fjord the water depth quickly increases to a depth of above 200 m (Figure 4). Within Nordfjord, a fjord basin in the inner part, and the sea floor surface appears generally smooth. There is nevertheless, the presence of several sediment lobes and a slide scar within the middle part of Nordfjord (Olsen, 2015).

In the intersection of Nordfjord and Kaiser Franz Joseph Fjord, Evans et al., (2002) found a prominent shallow sill. Sills may be a result of overdeepening of the fjord relatively to the adjacent shelf due to glacial activity, and are normally found at the mouth of the fjord, or within the fjord separating several basins (Syvitski et al., 1987).

The middle-outer part of Kaiser Franz Joseph Fjord has a maximum depth of ~550 meters, and the outer fjord basin can be divided into three sub-basins. At the mouth of Kaiser Franz Joseph Fjord, the Fosters Bugt form a wide embayment. The maximum water depth is here 340 meters. On the inner part of the shelf, there is an elevated high, where the water depth is 235 meters, whereas the outer most part of the continental shelf shows water depths between 280 – 340 meter deep. From the elevated high, the shelf stretches for 110 km to the shelf break (Evans et al., 2002).

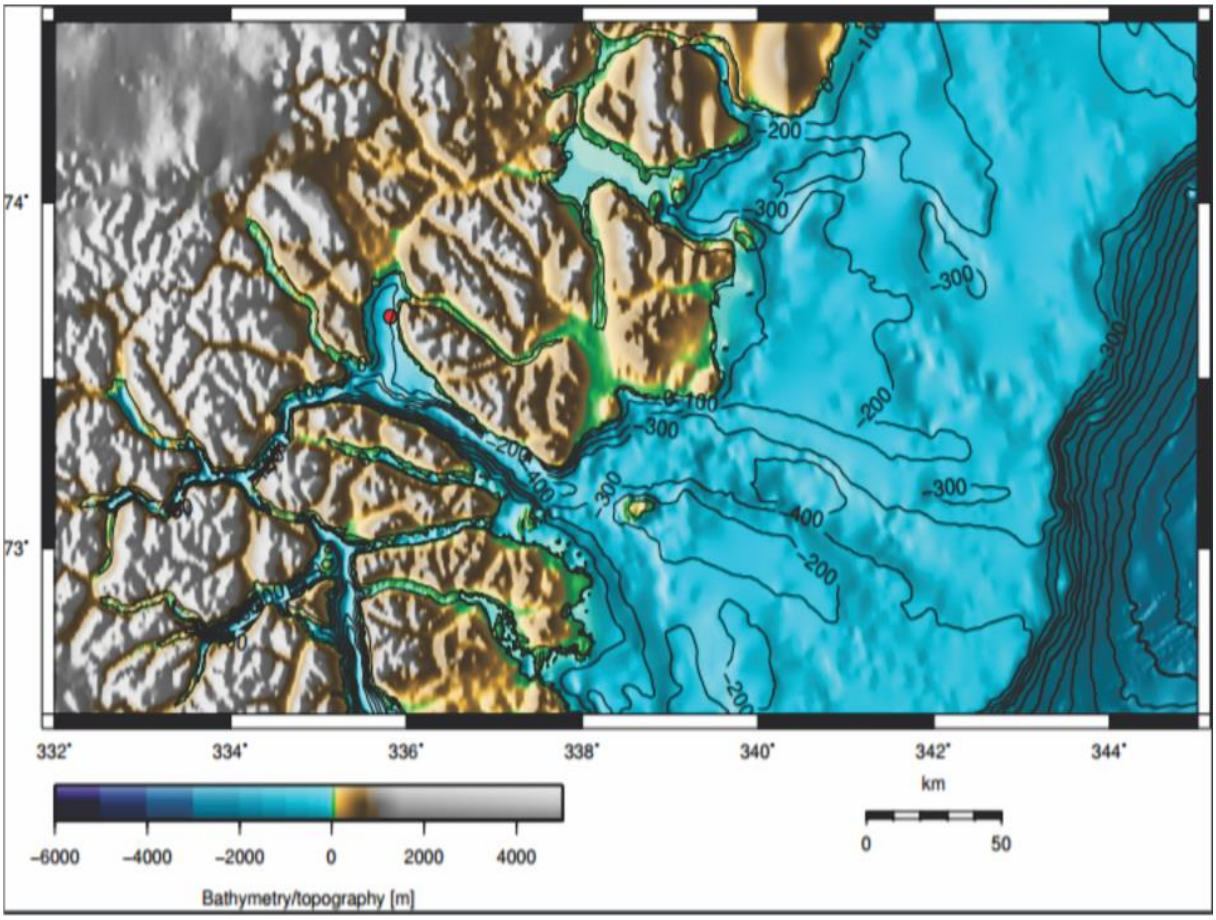

Figure 4: Bathymetric map of Kaiser Franz Joseph Fjord, and its associated continental shelf. Red dot indicates location of core HH13-012GC-TUNU.

2.3 Present oceanography

As mentioned, Eastern Greenland is majorly influenced by the EGC. The EGC originates at the Fram Strait and continues southwards along the East Greenland continental shelf and slope. As it reaches the

Denmark Strait, the EGC meets up with the warm Irminger Current, and continues around Cape Farewell and northwards along the western coast of Greenland (Figure 5).

Aagaard and Coachman, (1968) recognized three main water masses within the EGC north of Denmark Strait. The uppermost ~150 m consists of cold Polar Water (PW), which holds a temperature between ~0˚C and freezing point. Downwards in the PW, there is an increase in salinity from approximately 30ppt at the surface, to approximately 34ppt at the bottom. The middle water mass consists of Atlantic Intermediate Water (AIW), which extends down to ~800 meter below the sea surface. AIW has a temperature that is above 0˚C, and the salinity increases downwards from the top until it reaches a salinity between 34.88ppt-35ppt. This value is normally found above 400 m. From this depth, down to the base of the AIW, the salinity remains stable. The lowermost water mass is the Deep Water, which underlies the AIW. It holds a temperature below 0˚C, and a salinity between 34.87ppt - 34.95ppt.

However, it is not only water that is transported by the EGC. Substantial amounts of sea ice are also transported southwards along the East Greenland coast by the EGC. Outlet glaciers on the east coast of Greenland add icebergs and meltwater to the EGC during the summer months, but from October until June the drift is prevented by shore fast ice (Evans et al., 2002). The Greenland Ice Sheet is seen as one of the most important sources of freshwater to the North Atlantic, and the transport of meltwater from the glaciers, via fjords, into the oceanic system, is thereby an important process (Cottier et al., 2010).

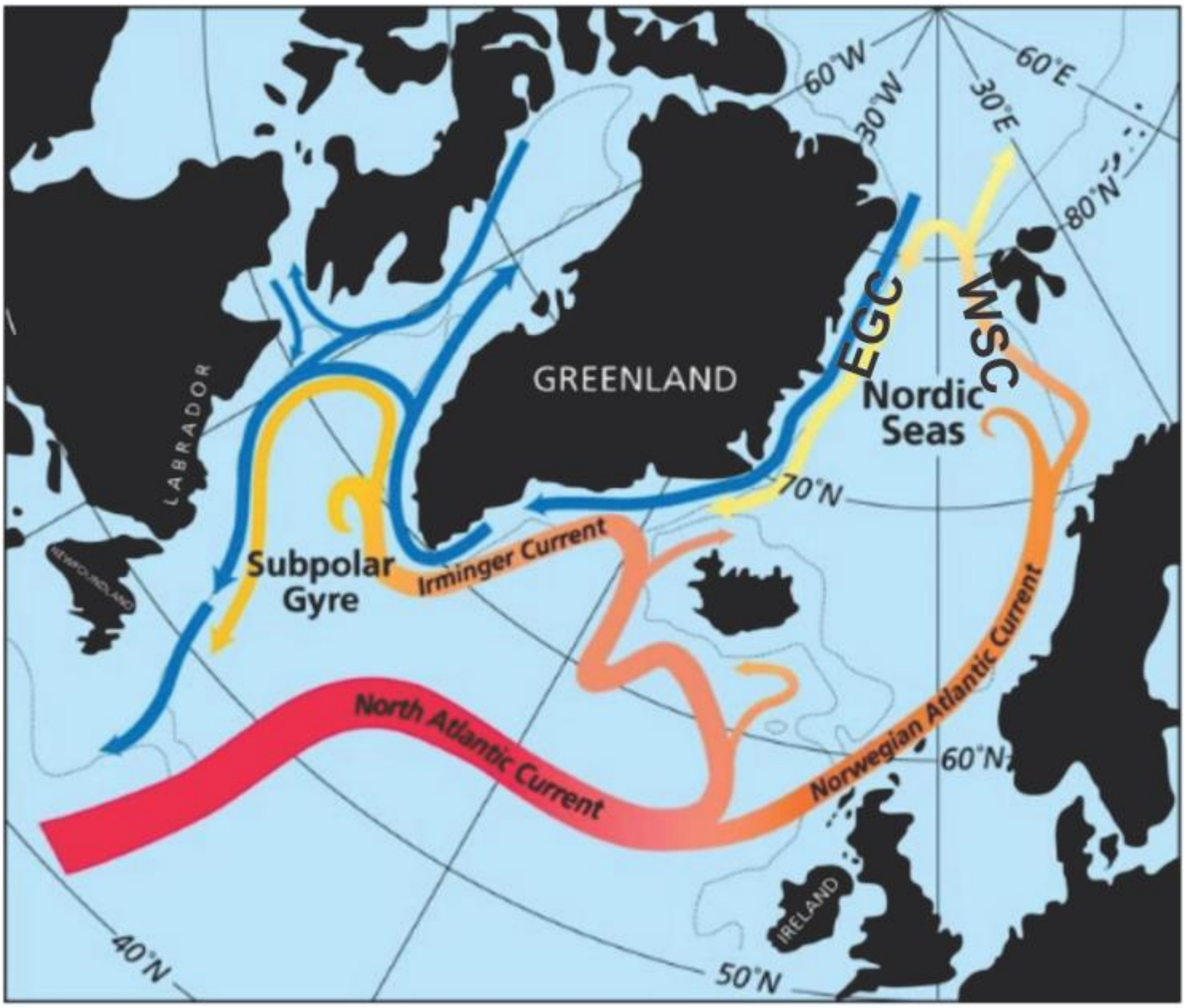

Figure 5: Present day ocean circulation in the Nordic Seas and North Atlantic. Blue arrows indicate flow path of cold and low saline PW, whereas the other arrows indicate flow path of warm and saline AW. Modified from Watts, (2010)

The general fjord circulation consists of surface water flowing from the head to the mouth of the fjord, and due to this movement, there is a current of inward moving water to balance the water budget in the fjord. There are several factors influencing the circulation in a fjord together with the bathymetry and the Coriolis Effect (Syvitski et al., 1987). According to Farmer and Freeland (1983), there are two main groups of factors influencing fjords. The first, “Buoyancy sources”, includes amongst other river discharge, the gravitational circulation, and the exchange of surface heat or water. The second, “Turbulent kinetic energy sources” includes tides, winds, convection by surface cooling and kinetic energy from rivers.

Within fjords with a sill, as Nordfjord has, there is a typical three layer arrangement of the water masses (Farmer and Freeland, 1983; Cottier et al., 2010). According to Cottier et al., (2010) the uppermost layer, the surface layer, consists of fresh water, which has its origin from melting of glaciers, basal melting or terrestrial runoff like rivers or melting of snow. The intermediate layer normally consists of advected water masses, which has its origin external to the fjord. Due to mixing with adjacent waters, the characteristics of the water masses are majorly altered from their original characteristics. As the EGC is the major transport force of water masses on the eastern coast of Greenland, the intermediate layer within the fjords is derived from the EGC, and is termed Polar Water (Cottier et al., 2010). The lowermost water masses typically consist of dense water with higher salinity than the overlying water masses. In the fjords of East Greenland, this water mass is made up of recirculated Atlantic Water from the Nordic Seas, or AW that has evolved into Arctic Intermediate Water (ArIW) (Azetsu-Scott and Tan, 1997; Cottier et al., 2010).

As Kaiser Franz Joseph Fjord is covered with sea ice during most of the year, year around oceanographic observations are not available. Hubberten, (1995) suggests that the interannual variability of both temperature and salinity is strong within the uppermost layer. This theory is based on comparison to other hydrographic stations on East Greenland. Within Nordfjord, the water inside and below sill depth is only renewed during certain periods of the year. In the other periods with no renewal, the water is stagnant, and the density is decreased over time as a result of vertical diffusion (Stigebrandt, 1976).

3. Material and Methods

3.1 Sediment Core

The sediment core, HH13-012-GC-TUNU, investigated in this project was collected during a scientific cruise with R/V Helmer Hanssen in august 2013. Station HH13-012-GC-TUNU is located at 73°40.515'N 024°10.939'E, and the core was retrieved from a water depth of approximately 210m. A total of 459 cm of sediments were preserved within the core. After retrieving the core on board the vessel, it was split into five sections, making up approximately 100 cm each.

3.2 Laboratory work

The laboratory work was carried out from May 2016, until December 2016 at the Department of Geoscience at The Arctic University of Norway in Tromsø.

3.2.1 Previous work

Olsen (2015) investigated the core to reconstruct the glacial history and sedimentary paleoenvironment in her master thesis. Her work included amongst other a grain size analysis, analysing the wet-bulk density and magnetic susceptibility, and doing a radiocarbon dating on the core. After her work, the core had been stored in cooling store with a temperature of approximately 4°C until the work on this project started.

3.2.2 Sampling

At every 5 cm of the core, a 1 cm thick slice was sub-sampled for foraminiferal analysis using a knife and a small spatula. After retrieving the slices, they were immediately put into plastic bags marked with the core name, and sampling depth. A total of 91 samples were retrieved from the core. After retrieving the samples from the core, they were stored in a cold storage over the summer.

In August 2016, every sample was weighed to establish the wet weight, before being left in the freeze dryer overnight. The freeze dryer efficiently removes water from within the sample by freezing the material and thereafter reducing the pressure, which leads to the sublimation of the water. After this process, it was possible to establish the dry weight of each sample the next day.

3.2.3 Sieving

Each of the samples were wet-sieved thoroughly through three sieves with mesh sizes of 1 mm, 100 µm, and 63 µm, thereby filtering out all of the clay in the samples. The 100 µm and 63 µm grain size fractions were sorted in previously labelled paper filters, whereas the 1 mm grain size fraction was kept in larger metal bowls. The paper filters and bowls were dried in a heating oven set to 40ºC, before weighing each grain size fraction.

3.2.4 Foraminiferal analysis

Foraminiferal analysis was at first made from every second sample within the 100µm size fraction, making up 45 samples. When all of these were analysed, a total of 25 extra samples were counted. These extra samples were chosen as they were located in transition zones within the core. Most of the samples were small enough to use the entire 100µm size fraction when counting, but some of them contained too much material for it all to be counted at the same time. These samples were split into two equal parts using a manual sample splitter.

In theory at least 300 calcareous benthic foraminifera within each sample should be picked and identified from a picking tray, using a microscope, to get a reliable statistic. However, only 24 samples contained over 300 calcareous benthic foraminifera, whereas the number of specimens in the other samples varied between 50 and 290 specimens. In the final statistics, only the 57 samples containing more than 100 specimens are included in order to get the most credible statistics. In addition, both the planktic and agglutinated foraminifera found within the same squares as the benthic foraminifera were identified. Species identifications were made by comparing the observed foraminifera with foraminifera plates found within Feyling-Hanssen (1964), and using the Ellis & Messina Catalogue of Micropaleontology, as well as comparing them to foraminifera species slides found in the laboratory.

3.2.5 Foraminiferal concentration and flux calculations

After identifying the necessary 300 foraminifera from the sample, the percentage abundance of each species was calculated by dividing it by the total amount of benthic foraminifera found within the picked sample:

$$Percentage\ abundance = \frac{Number\ of\ speciemens\ of specie\ X}{Total\ number\ of\ benthic\ foraminifera} * 100\%$$

The foraminiferal flux was calculated by the following formula:

$$Foraminifera\ flux = foraminifera\ concentration * bulk\ density * sedimentation\ rate$$

For bulk density, the mean wet bulk density given by Olsen, (2015) (1,8 g/cm^3) is chosen, as there was not enough data available to calculate the dry bulk density. This leads to a consequent use of wet weight throughout the calculations for foraminiferal flux.

The foraminiferal concentration within a sample is calculated by the relative amount of foraminifera divided by the total wet weight:

$$Concentration = \frac{\left(\left(\frac{Number\ of\ Foraminifera}{Squares\ counted}*45\right)*number\ of\ splits\right)}{Wet\ weight\ sediment}$$

3.2.6 Radiocarbon dating and calibration

During her work, Olsen (2015) radiocarbon dated the core. Three samples were collected, located at 455-454 cm, 196-195 cm, and 98-97 cm, whereof only the two deepest samples contained enough material to be radiocarbon dated (Table 1).

3.2.6.1 Principle

Radiocarbon dating is a method based on the decay of ^{14}C, which is a radioactive isotope found within the atmosphere. By assuming that the ratio between ^{14}C and ^{12}C within the atmosphere has been constant during time, and knowing the half life time of ^{14}C (5730 ± 30years), organisms containing organic material can be dated by comparing the residual $^{14}C/^{12}C$ ratio to the modern standard (Allaby, 2013). Due to the known half-life time, this method is useful up to approximately 50 000 years, before all ^{14}C within the samples have decayed.

3.2.6.2 Calibration and marine reservoir effects

As a result of variations in atmospheric ^{14}C concentration values through time, due to changes in production rates, ^{14}C years do not directly transfer to calendar years. To get the age in calendar years, it is necessary to make a calibration (Reimer et al., 2013a).

At the sea surface, there is a constant exchange of ^{14}C from the atmosphere to the sea. However, this exchange only occurs at the sea surface, and does not occur deeper in the sea. As water masses sink from the sea surface, the exchange stops, and the ^{14}C isotope will start to decay. As a result of this, the apparent age of the water mass increases. This effect is called the marine reservoir effect, and the average global marine reservoir age is ~400 years (Mangerud, 1972; Reimer et al., 2013b). Another factor to take into account is the local regional difference (ΔR). The ΔR varies over short distances, and is due to regional differences of the different water masses (Stuiver and Braziunas, 1993).

To calibrate the radiocarbon ages obtained from Olsen (2015) to calendar years Before Present, the CALIB 7.1 software was used. This software uses the MARINE13 curve, and a global reservoir correction of 405 years (Reimer et al., 2013a). As this does not take the regional differences into account, an extra ΔR of 166 ± 54 was used (Haakansson, 1973).

Table 1: Calibrated ages

Lab reference	Sampling depth (cm)	^{14}C age BP	Cal. yr. BP Calib 7.1 1 σ range	Cal. yr. BP Calib 7.1 2 σ range	Cal. yr. BP Calib 7.1 Median Probability
60281.1.1	195 cm	1295 ± 70	614-777	537-871	691
60282.1.1	454 cm	7470 ± 130	7644-7911	7500-8036	7771

3.2.7 Age model

An age model was established by using linear interpolation between the calibrated ages obtained from radiocarbon dates from Olsen (2015), and assuming an age of 2013CE of the upper 10 cm. By assuming that the sediment accumulation rates within the core area had stayed constant between the dated intervals in the core, the age at different depths can be estimated by applying the formula for a linear equation:

$$y = ax + b$$

In this case, only two of the radiocarbon samples contained enough material to be dated. Moreover, it cannot be ratified that there has not been a change in the accumulation rates of sedimentation either between these two depths, or after. This will be discussed in Chapter 4.1.

4. Results

4.1 Age model

As there are only two dated levels within the core (454cm and 195cm), the age model (Figure 6) is established by assuming a constant sedimentation rate between these two levels. Olsen (2015) discovered several muddy sand layers between the two dated levels (Figure 7). These layers might be turbidites which can erode, and remove sediments. It is therefore difficult to claim with certainty that the sediments between the two dated levels have not been disturbed, and that the sedimentation rate has been constant. On the other hand, a linear sedimentation rate is the best option with the data available.

As there was no radiocarbon dating done above 195 cm within the core, the sedimentation rate between 195cm-0cm is unknown. Two main theories were considered when establishing the age of the upper 195 cm.

The first theory that was considered, was a linear sedimentation rate throughout the entire core, following the same trend as between the two dated levels. This would on the other hand, give an assumed age at the uppermost part, of approximately 4000 years into the future. If the sedimentation rate has stayed constant throughout the entire core, there must be one or several hiatuses present within the core. However, in her work, Olsen (2015) discovered that the uppermost 50 cm of the core most likely accumulated in less than 100 years, which gives a much higher sedimentation rate in the uppermost part than between the two dated levels, indicating a change in sedimentation rate through the core.

The second theory that was considered, the one that was chosen for the age model presented in Figure 6, was an age model with a change in sedimentation rate. The 10 cm sample is assumed to represent the year of retrieval (2013 CE). This assumption is made as Olsen (2015) described that the uppermost 10 cm of the core was heavily disturbed during core retrieval. As seen from the age model, this theory gives an abrupt rise in sedimentation rate in the upper 195 cm. The presumption that the uppermost 50 cm most likely accumulated during less than 100 years, could support the theory presented in the age model.

The accumulation rates between the dated levels are presented in Table 2. In Appendix 1 the calibrated ages, both the ones used for the age model, including a change in accumulation rate, and those of the theory of a linear sedimentation rate throughout the entire core are visualized.

Table 2: Accumulation rate throughout core HH13-012GC-TUNU.

Depth (cm)	Age (cal. yr. BP)	Accumulation rate (cm/k yr.)
454 – 195	7771 – 691	36
195 – 10	691 – -63	279

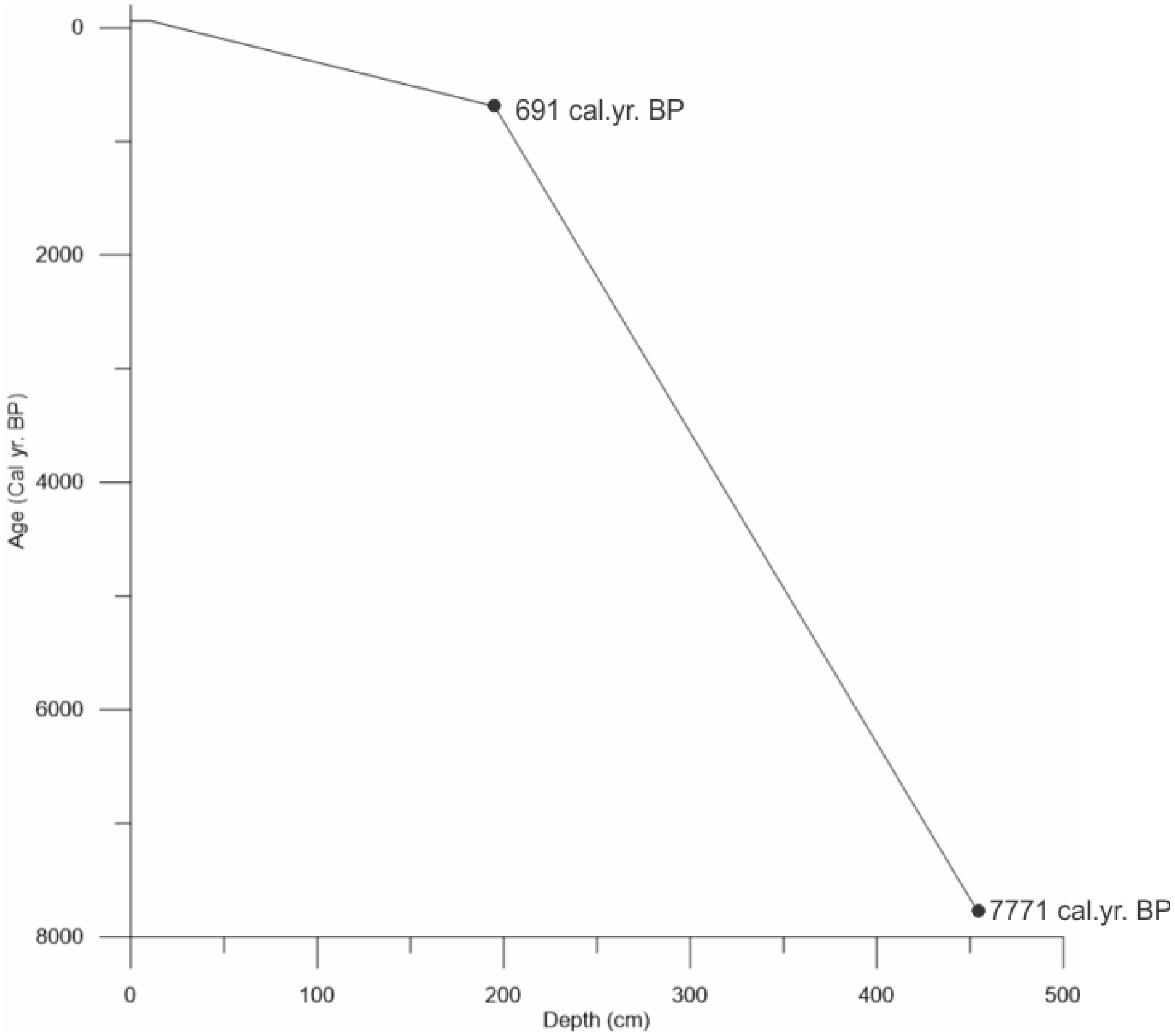

Figure 6: Age-depth plot for HH13-012GC-TUNU. The black dots indicate the levels within the core that were radiocarbon dated, and their calibrated ages.

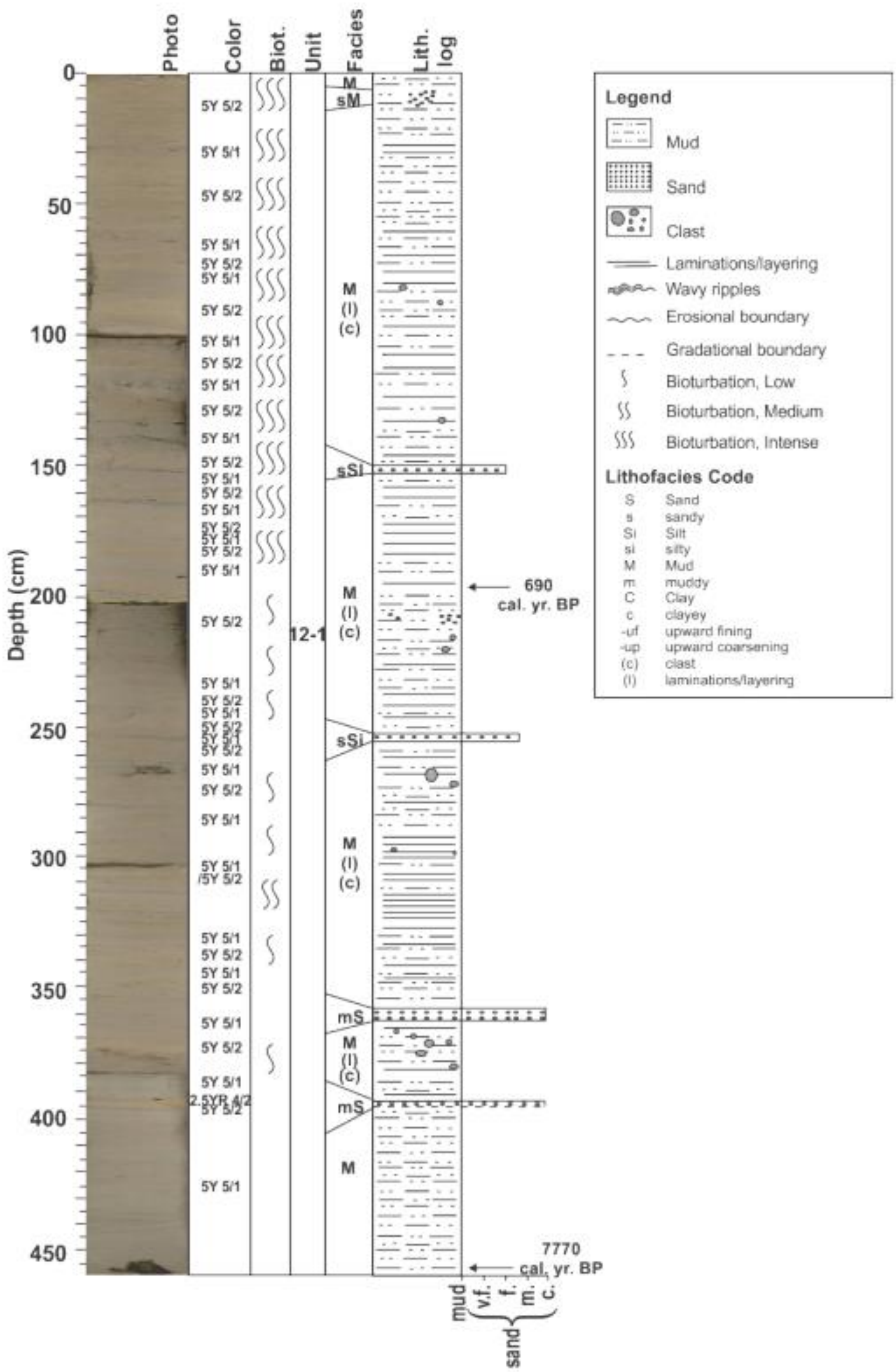

Figure 7: Lithological log of core HH13-012GC-TUNU. (Adapted from Olsen (2015))

4.2 Foraminifera

As seen from Table 3, a total of 24 different calcareous species of benthic foraminifera were identified within the core, in addition to five different agglutinated species. Overall there were no clear indications of dissolution of the calcareous foraminifera. Of the 29 benthic species, 10 occurred with a high enough relative abundance (>2%) to be taken into account when considering the results.

The total number of benthic calcareous species, agglutinated species, and planktic species at each sampling depth is seen in Appendix 2, whereas the number of each identified species within each sample is found in Appendix 3.

Table 3: Foraminiferal list including all benthic calcareous, and agglutinated species found within core HH13-012GC-TUNU.

SPECIES LIST
Benthic species
***Astrononion gallowayi* Loeblich & Tappan, 1953**
***Cassidulina laevigata* Rhumbler, 1949**
***Cassidulina reniforme* Nørvang, 1945**
***Cassidulina teretis* Tappan, 1951**
***Cibicides lobatulus* (Walker & Jacob, 1798)**
***Dentalina drammenensis* (Feyling-Hanssen, 1964)**
***Dentalina trondheimensis* (Feyling-Hanssen, 1964)**
***Elphidium excavatum* f. *clavata* Cushman, 1930**
***Elphidium hallandense* Brotzen, 1943**
***Fissurina laevigata* Reuss, 1850**
***Globobulimina sp.* Cushman, 1927**
***Haynesina orbiculare* (Brady, 1881)**
***Islandiella helenae* Feyling-Hanssen & Buzas, 1976**
***Islandiella norcrossi* (Cushman, 1933)**
***Lagena clavata* (d'Orbigny, 1846)**
Lenticula linearis
***Melonis barleeanus* (Williamson, 1858)**
***Parafissurina lateralis* (Cushman, 1913)**
***Quinqueloculina stalkeri* Loeblich & Tappan, 1953**
***Stainforthia fusiformis* (Williamson, 1848)**
***Stainforthia loeblichi* Feyling-Hanssen, 1954**
***Silicosigmoilina groenlandica* Loeblich & Tappan, 1953**
***Triloculina tricarinata* d'Orbigny, 1826**
***Triloculina trihedra* Loeblich & Tappan, 1953**
Agglutinated species
***Adercotryma glomeratum* (Brady, 1878)**
***Alveolophragmium crassimargo* (Norman, 1892)**
***Textularia earlandi* Parker, 1952**
***Cribrostomoides crassimargo* (Norman, 1892)**
***Jadammina macrescens* (Brady, 1870)**

4.2.1 Ecological preferences of dominating species

Different foraminifera thrive within different environments, which can be of great importance for the interpretation of the past environment. As mentioned, 10 different species occurred with a high enough abundance to be taken into account while considering the results. Their ecological preferences are discussed in alphabetical order in the following sub-chapters.

4.2.1.1 *Astrononion gallowayi*

Astrononion gallowayi is a facultative epifaunal species that seems to prefer shallow areas related to coarse sediments, and high current conditions (Steinsund et al., 1994; Polyak et al., 2002). According to Steinsund et al., (1994), the species prefers low temperatures (< 1°C) and high salinities above at least 30‰, and preferably above 33‰. Wollenburg and Mackensen, (1998) claim that the species also can occur as an infaunal species. When *A. gallowayi* is found within muddy sediments, and especially combined with the occurrence of *Cibicides lobatulus*, it may be an indicator of post-mortem transport (Husum and Hald, 2004; Jennings et al., 2004).

4.2.1.2 *Cassidulina reniforme*

This species is frequently found in glaciomarine environments, and it is one of the most commonly found species on the Arctic shelves (Hald and Korsun, 1997; Polyak et al., 2002). Steinsund et al., (1994) claim that *C. reniforme* is an opportunistic species taking advantage of environments that generally are unfavourable. The species prefers areas with water temperatures below ca. 2°C, in addition to seasonal ice cover, and preferably muddy sediments. As for the salinity conditions, the species is seldom found in areas with a salinity below 30‰ (Steinsund et al., 1994; Polyak et al., 2002). *C. reniforme* is often described as ice-proximal, as the species seems to be abundant close to glacier terminus (Hald and Korsun, 1997).

4.2.1.3 *Cibicides lobatulus*

Cibicides lobatulus is a species that, like *A. gallowayi*, thrives in environments with high energy conditions, coarse sediments and a low sedimentation rate (Steinsund et al., 1994; Hald and Korsun, 1997; Polyak et al., 2002). *C. lobatulus* is described as an epifaunal suspension feeder, which often clings on to coarse material in the high energy conditions (Steinsund et al., 1994; Hald and Korsun, 1997; Polyak et al., 2002). Ivanova et al., (2008) discovered that the species can penetrate deep into sediments by being transported downwards by bioturbation. The species is tolerant to a wide range of temperatures, but is more particular about salinity, where it prefers salinities above 32‰ (Steinsund et al., 1994).

4.2.1.*4 Elphidium excavatum* forma *clavata*

Elphidium excavatum forma *clavata* is the most common shallow marine benthic foraminifera found within late Quaternary glaciomarine deposits from the Arctic shelves (Steinsund et al., 1994; Hald and Korsun, 1997). The species is widely distributed on Arctic shelves and shallow polar seas, and is often found in extreme conditions, as near-glacial environments (Hald and Korsun, 1997; Polyak et al., 2002). Near-glacial environments are known for strongly fluctuating environmental conditions, with rapid changes in salinity and sediment supply, and *E. excavatum f. clavata* is thereby considered an opportunistic species (Hald and Korsun, 1997; Jennings et al., 2004). Within these areas that are seeming unsuitable for life, the species is capable of quickly colonizing the seafloor as a result of being nutritional and habitat versatile (Linke and Lutze, 1993; Steinsund et al., 1994; Polyak et al., 2002). Steinsund et al., (1994) claim that the species thrives in areas with fluctuating temperatures, preferably below 1℃, and a salinity range from 30-34‰, as well as high energy conditions, high sedimentation rates, and the presence of sea ice.

4.2.1.5 *Haynesina orbiculare*

Haynesina orbiculare is a species that can indicate shallow water depths and the species can often be found in areas with cold water and stable marine salinities (Hansen and Knudsen, 1995; Polyak et al., 2002). In addition, according to Polyak et al., (2002), *H. orbiculare* can be a major indicator of river-proximal environments.

4.2.1.6 *Islandiella helenae*

Islandiella helenae is an Arctic species that thrives in open ocean with stable salinity (Hald and Korsun, 1997). As the species is an open-ocean form, according to Korsun and Hald, (1998) *I. helenae* is also an indicator of glacier-distal environments. Steinsund et al., (1994) do on the other hand claim that the species populates areas that are shallow and have a less stable environment.

4.2.1.7 *Islandiella norcrossi*

Korsun and Hald, (1998) claim that *I. norcrossi* has its main distribution in cold waters on the Arctic shelf, and prefers relatively high and stable bottom water salinities. This contention is supported by Steinsund et al., (1994) who say that the species thrives in areas with relatively low temperature, and relatively high salinities. The authors also claim that mixed populations between *I. norcrossi* and *I. helenae* are common in shallow areas with unstable environments. Others indicate that the species has its preferred environment at water depths from 200-400 m, preferring fine sediments, and low sedimentation rates, in addition to seasonal sea ice (Steinsund et al., 1994; Polyak et al., 2002).

4.2.1.8 *Quinqueloculina stalkeri*

According to Korsun and Hald, (1998) *Quinqueloculina stalkeri* is an Arctic species that occurs in shallow waters surrounding Alaska, Greenland, and Svalbard. The authors say that the species might be an indicator of near-glacier, shallow marine habitats, as it is very rarely, or not at all, found in the Late glacial deposits in areas with deeper water.

4.2.1.9 *Stainforthia loeblichi*

Stainforthia loeblichi is a species that mainly occurs in cold waters (~0°C) and areas influenced by seasonal sea ice (Steinsund et al., 1994). According to Polyak et al., (2002) the *Stainforthia* species is opportunistic, and takes advantage of pulses of high seasonal productivity. *S. loeblichi* is an infaunal species according to Wollenburg and Mackensen, (1998).

4.2.1.10 *Triloculina tricarinata*

Very little is known about this species. However, some research indicate that it can live in environments with salinities up to 38‰ (Dias et al., 2010). In addition, the species is found within fine sandy mud (Wang and Chappell, 2001), and in the North Atlantic it is observed at water depths below 2400 meters (Hermelin and Scott, 1985).

4.3 Foraminiferal assemblage zones

Three assemblage zones are defined within HH13-012GC-TUNU (Figure 8 and Figure 9). Normally, the foraminiferal flux would be taken into as much account as the percentage abundance of foraminiferal species when establishing the boarders between the different zones. However, as the flux is related to the sedimentation rate, which in this case is not very reliable due to only two dated levels, the assemblage zones established in this research are mainly based on the percentage abundance of the species.

The relative abundance of each species can be seen in Appendix 4, and the total benthic calcareous foraminiferal flux can be seen in Appendix 5.

4.3.1 Establishment of assemblage zones

Three different assemblage zones have been identified and are named AZ 1, AZ 2 and AZ 3, where AZ 3 is located at the bottom of the core, and AZ 1 at the top. As seen from Figure 8, AZ 3 stretches from 454 – 360 cm, AZ 2 stretches from 360 – 180 cm, and AZ 1 stretches from 180 – 0 cm. The border between AZ 3 and AZ 2 is established by the decrease in percentage abundance of *I. helenae* towards the border, combined with the sudden increase of *A. gallowayi* when entering the deepest part of AZ 2. In addition, there are near the borderline in AZ 3, peak high of *H. orbiculare, S. loeblichi,* and *C. lobatulus.* The border between AZ 2 and AZ 1 at 180 cm, is established by the major increase of *E. excavatum* f. *clavata* in the lowermost part of AZ 1 as well as the decrease of *A. gallowayi*. By looking at the age model, AZ 3 covers 7771 – 5201 cal. yr. BP, AZ 2 covers 5201 – 630 cal. yr. BP, and AZ 1 covers 630 - -63 (2013 CE) cal. yr. BP (Figure 9).

4.3.2 Assemblage zone 3 (AZ 3)

AZ 3 is located from 454 – 360 cm when the results are plotted against depth, and 7771 – 5201 cal. yr. BP when plotted against age (Figure 8 and Figure 9).

C. reniforme and *I. helenae* are the dominating species within this assemblage zone. The abundance of *C. reniforme* is quite stable throughout the entire zone, with a slight decrease from the bottom, towards the top of the zone. The maximum abundance is ~66%, and the minimum is ~37%, with an average of ~55%. The frequency of *I. helenae* increases slightly from the bottom of the assemblage zone, until it reaches its maximum value of ~47% at 365 cm (5338 cal. yr. BP). Following this maximum, there is a decrease in the abundance of the species towards the border to AZ2. The species constitutes on average ~29% of the assemblage zone.

The relative abundance of *E. excavatum* f. *clavata* is, as *C. reniforme*, relatively stable throughout the zone, reaching a maximum of ~21% at 435 cm (7252 cal. yr. BP). The species constitutes on average 7,5% of the assemblage zone. The percentage of *A. gallowayi* stays low throughout the entire zone, with an average value below 0,5%, and it increases slightly towards the upper part of the assemblage zone. The frequency of *C. lobatulus* varies from 0-1% within the assemblage zone except for the interval around 385 cm (5885 cal. yr. BP) where it reaches a high value of 14%. The abundance of *Q. stalkeri* and *T. tricarinata* are both low throughout most of the assemblage zone, and do not exceed 1%. The relative abundance of *I. norcrossi* and *S. loeblichi* show generally the same trends within AZ 3, with relatively high values in the lower and upper part of the zone. The average percentage of *I. norcrossi* is ~0,5%, whereas the average of *S. loeblichi* is ~1,6%. *H. orbiculare* does not occur before 365 cm (5338 cal. yr. BP), where it reaches its maximum percentage of ~4,6%. *H. orbiculare* has an average abundance of ~0.5%.

The total benthic calcareous foraminiferal flux within AZ 3 is characterized by two areas with relative high values, at 425 - 395 cm (6978 – 6158 cal. yr. BP) and 375 – 365 cm (5612 – 5338 cal. yr. BP). It reaches its maximum value of ~4800 specimens/cm^2/year at 365 cm. The average foraminiferal flux within the zone is 2192 specimens/cm^2/year.

4.3.3 Assemblage zone 2 (AZ 2)

AZ 2 is located from 360 – 180 cm when the results are plotted against depth, and 5201 – 630 cal. yr. BP when plotted against age (Figure 8 and Figure 9). *C. reniforme* is, as in AZ 3, the dominating species within the assemblage zone. It increases slightly from the bottom of the zone, until it reaches its maximum value of 73% at 265 cm (2605 cal. yr. BP). Following this maximum, there is a drop in the abundance, reaching a minimum value of ~34% at 215 cm (1238 cal. yr. BP). Following this minimum, there is a slight increase in the abundance towards the top of the zone. *C. reniforme* constitutes on average ~51% within AZ 2.

The relative abundance of *A. gallowayi* is, opposite to in AZ 3, relatively high within AZ 2. From the bottom of the zone, the percentage rises up to ~36%, followed by a drop, and a new increase, before it stabilizes with values all above 15%, still including some fluctuations. Above 215 cm (1238 cal. yr. BP) there is a general decrease in the relative abundance towards the top of the zone. Maximum high, ~43%, is found at 235 cm (1784 cal. yr. BP), and the average of the species is ~20%. The abundance of *E. excavatum* f. *clavata* fluctuates throughout the zone, starting off with a high value at 300 cm (3561 cal. yr. BP), exceeding 34%, followed by a period with barely no presence until 250 cm (2195 cal. yr. BP), where four relatively high values can be observed, intervened with abrupt decrease between each. The maximum high of ~42% is found at 210 cm (1101 cal. yr. BP). Following this high value, the relative abundance decreases to ~0,1% just below the assemblage zone border. The species average percentage within AZ 2 is ~12%.

I. helenae, which was quite abundant within AZ 3, shows a general decrease in relative abundance from the bottom of the zone towards the top. Its maximum value is ~26%, and the minimum value is ~1%, making up an average percentage throughout the zone of ~7%. The percentage of *Q. stalkeri* fluctuates throughout the zone, with a slight increase in the middle of the zone. The maximum value is found at 346 cm (4819 cal. yr. BP), where it exceeds 10%. Elsewhere in the zone the relative abundance varies from 0% - ~9%. The species average abundance is ~2,9%. *T. tricarinata,* and *I. norcrossi* follow approximately the same trend with fluctuations including several peaks throughout the zone. *T. tricarinata* is reaching a maximum at 335 cm (4518 cal. yr. BP), with a relative abundance of ~9%, whereas *I. norcrossi* reaches a maximum at 185 cm, where the relative abundance exceeds 2%. The average percentage of the two species are respectively ~2% and ~0,5%. The relative abundance of *S. loeblichi* is generally low through AZ 2, with relative high values in the intervals 265 - 255 cm (2605 – 2331 cal. yr. BP), and 210 cm (1101 cal. yr. BP) where it exceeds 1,5 %. Other than these areas, the relative abundance is <1%, which gives an average percentage of ~1,2%. The percentage of *H. orbiculare* is also low through the zone. It reaches its maximum value at 210 cm (1101 cal. yr. BP), where the relative abundance is 1,7%, otherwise it is <0,9%, making up an average abundance of ~0,8% within AZ 2. *C. lobatulus* is only observed at two different depths, at 285 cm (3151 cal. yr. BP) and 240 cm (1921 cal. yr. BP), with values of respectively 0,4% and 0,3%.

The total benthic calcareous foraminiferal flux within AZ 2 is low throughout the entire zone, with an increase in the values at the uppermost part. On average the foraminiferal flux is 585 specimens/cm^2/year.

4.3.4 Assemblage zone 1 (AZ 1)

Assemblage zone 1 is located from 180 cm – 0 cm when plotted against depth, and from 630 – -63 cal. yr. BP (2013CE) when plotted against age (Figure 8 and Figure 9). *C. reniforme* and *E. excavatum* f. *clavata* are the most common species within this assemblage zone. *C. reniforme* appears to fluctuate cyclically with several high values exceeding 57 %, intervened by low values down to 25%. The maximum abundance is located at 40 cm (59 cal. yr. BP), where it exceeds 64%, and the minimum is located at 165 cm (569 cal. yr. BP), where it is 25%. The average percentage of *C. reniforme,* within the zone is ~49%. The percentage of *E. excavatum* f. *clavata* increases from barely being present at the borderline between AZ 2 and AZ 1, up to above 40% at 165 cm (569 cal. yr. BP). Through the zone, the species, as *C. reniforme*, fluctuates with high values and intervening low values. It exceeds 45% at both 125cm (406 cal. yr. BP), and 70 cm (182 cal. yr. BP). The maximum abundance, ~48%, is found at 125 cm (406 cal. yr. BP), and the minimum is ~15% at 15 cm (-43 cal. yr. BP / 1993CE). The average of the species is ~31%. It is worth noticing that several of the high values of *E. excavatum* f. *clavata* coincide with lower values of *C. reniforme,* and vice versa.

Compared to the results in AZ 2, *A. gallowayi* has a lower relative abundance within AZ 1, decreasing from the bottom of the zone, towards the top. The maximum value is located at 165 cm (569 cal. yr. BP), where it makes up ~27% of the total fauna. The average percentage of *A. gallowayi* within the zone is ~10%. *Q. stalkeri* shows a general increase in the relative abundance from 0% at the assemblage zone border, up to approximately 11% at 25 cm (-2 cal. yr. BP / 1952CE), before it decreases slightly at the top of the zone. The average of the species is ~5%. *I. helenae* continues the low values found within AZ 2, and makes up an average of ~1,2%. Both *I. norcrossi*, and *S. loeblichi* fluctuate heavily through AZ 1. *I. norcrossi* shows a trend of increased values in the middle of the zone, with low values at both the bottom and top. The average abundance of the two species are ~0,75% for both. *T. tricarinata* shows rather a quite stable trend throughout the assemblage zone, with a slight decrease from the bottom towards the top. Some minor relatively high values can be observed, and the maximum abundance is ~3,9%, located at 155 cm (529 cal. yr. BP). The species' average abundance is ~1,4%. *H. orbiculare* does only occur at one level within AZ 1. At 165 cm (569 cal. yr. BP), it makes up ~0,3 % of the total foraminiferal fauna.

The total benthic calcareous foraminiferal flux within AZ 3 is fluctuating throughout the entire zone, with several high values intervened by following low values. The maximum value of ~4800 specimens/cm^2/year is found at 155 cm (528 cal. yr. BP). On average the foraminiferal flux within the zone is 2010 specimens/cm^2/year.

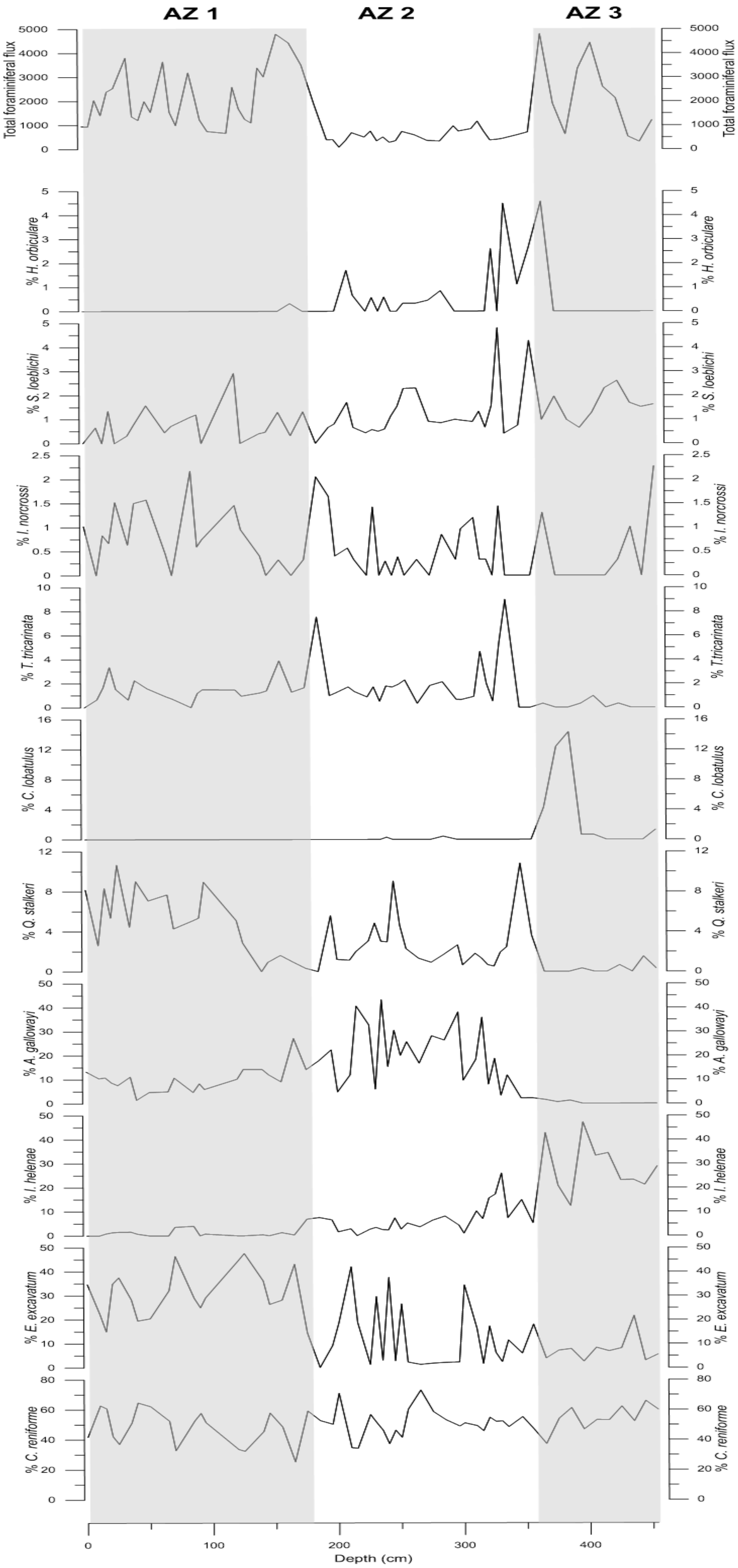

Figure 8: Percentage abundance of the most common species found within HH13-012GC-TUNU, in addition to the total benthic calcareous foraminiferal flux, plotted against depth, and the established foraminiferal assemblage zones AZ 1-AZ 3.

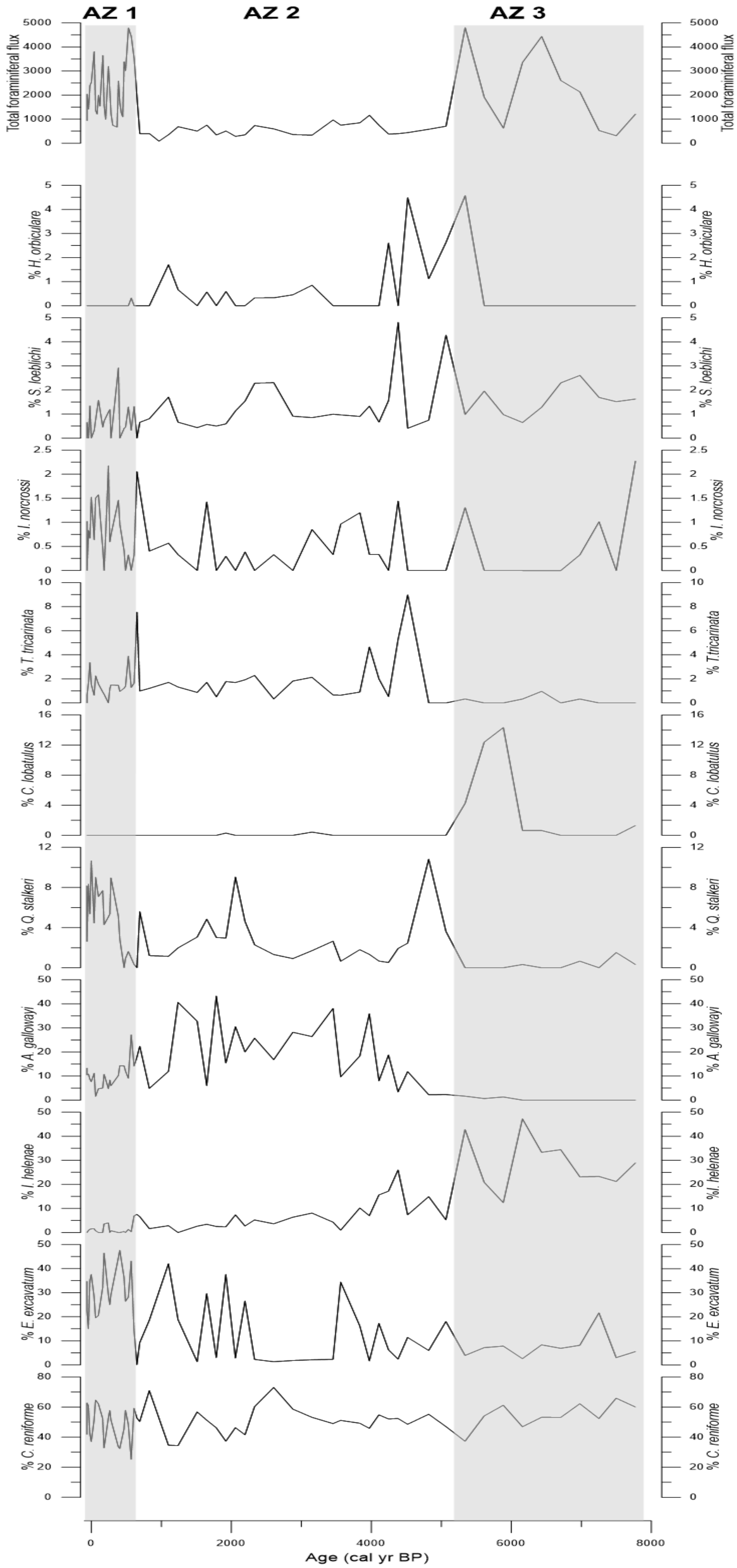

Figure 9: Percentage abundance of the most common species found within HH13-012GC-TUNU, in addition to total benthic calcareous flux, plotted against age, and the established foraminiferal assemblage zones AZ 1-AZ 3.

5. Discussion

5.1 Interpretation of assemblage zones

In the following sub-chapters, the paleoenvironment within each of the three assemblage zones will be interpreted based on the environmental preferences of the most abundant species.

5.1.1 Dissolution of calcareous foraminifera

Due to an increased solubility of CO_2 within colder water, dissolution of calcareous foraminifera is often observed within the cold and low-saline Arctic waters (Hald and Steinsund, 1992; Jennings and Helgadottir, 1994). Findings from the East Greenland shelf and in fjords located south of the study area in this study, suggest that the abundance of calcareous species is connected to water mass changes, including productivity, sea-ice cover and dissolution of $CaCO_3$ (Jennings and Helgadottir, 1994; Jennings and Weiner, 1996). Jennings and Weiner (1996) suggested a dissolution gradient with two end-members, where areas that were influenced by Polar Waters showed 100% calcareous dissolution, and areas influenced by Atlantic Intermediate Water showed 90 % preservation of calcium carbonate as the two end-members.

Findings from Disko Bugt, in West-Greenland, suggest a connection between dissolution of calcareous foraminifera and the sedimentation rate in areas in close proximity to a glacier. Periods with high sedimentation rates and cold water conditions favour preservation of calcareous foraminifera, and periods with low sedimentation rates and relative warm water conditions increase the dissolution of calcareous foraminifera (Lloyd et al., 2005; Lloyd, 2006).

Although there are several levels within core HH13-012GC-TUNU with low abundance of calcareous foraminifera, the samples showed little or no visual signs of dissolution. However, one cannot disembark the possibility of dissolution being a contributing factor.

5.1.2 Assemblage zone 3

The assemblage zone is dominated by *C. reniforme* and *I. helenae*. *C. reniforme* is a species thriving in cold bottom waters (<2°C), with salinities above 30‰, in addition to seasonal ice cover. The species can be an indicator of both glacier-proximal, and distal glaciomarine environments (Steinsund et al., 1994; Hald and Korsun, 1997; Korsun and Hald, 1998; Polyak et al., 2002). *I. helenae* is associated with seasonal ice cover (Steinsund et al., 1994), and thrives in areas with high and stable salinity(Korsun and Hald, 1998). The species is also known to be an indicator of glacier-distal environments (Korsun and Hald, 1998), and as the levels with the highest relative abundance of the species coincide with minor drops in relative abundance of both *C. reniforme* and *E. excavatum* f.

clavata it can be assumed that the environment is glacier-distal and influenced by Atlantic Water at these levels.

At 385 cm (5885 cal. yr. BP) *C. lobatulus* reaches its maximum value of 14%. This relative high value may indicate a period with a salinity above 32‰, combined with high energy conditions (Steinsund et al., 1994; Hald and Korsun, 1997; Polyak et al., 2002).

The maximum abundance of both *I. norcrossi* and *S. loeblichi* is below 5%. Due to the low relative abundance, the presence of these species in the lower and upper part of the zone cannot indicate any major environmental changes on their own. However, *S. loeblichi* can be an indicator of high seasonal productivity, and sometimes occurs in oxygen depleted environments. Moreover, high relative values of *H. orbiculare* can be indicative of stable marine salinities and cold water. In addition, the species may indicate shallow water depths (Hansen and Knudsen, 1995; Polyak et al., 2002).

The total foraminiferal flux is characterized by two areas with relative high values, at 425 - 395 cm (6978 – 6158 cal. yr. BP) and 375 – 365 cm (5612 – 5338 cal. yr. BP), indicating a favourable environment. Both levels coincide with relative high abundance of *I. helenae*, which aforementioned indicates a glacier-distal environment, and seasonal sea-ice cover. Seasonal sea-ice can enhance primary productivity at the sea-ice margin, and thereby an increased food supply for the foraminifera (Seidenkrantz, 2013; Ribeiro et al., 2017).

Generally the area within AZ 3 has been influenced by inflow of recirculated Atlantic Water up until ~390 cm (6022 cal. yr. BP), with seasonal sea ice affecting the area. During this period there is also an increase in the total foraminiferal flux, and there does not seem to be any major changes in energy conditions. Following this level, the introduction of *C. lobatulus* indicates a period (390 – 370 cm, 6022 – 5475 cal. yr. BP) of higher energy conditions. The general decrease in abundance of *I. helenae* from 365 cm (5338 cal. yr. BP) towards the top of the zone, may indicate that colder and less saline water masses are entering the fjord. Occurrence of the cold water species *E. excavatum* f. *clavata* towards the top of the zone can support this theory.

5.1.3 Assemblage zone 2

The relative abundance of *C. reniforme* is as high in AZ 2 as in AZ 3, meaning that the conditions still are those of a glaciomarine setting. The most noticeable change is the introduction of *A. gallowayi*, which is an indicator of high bottom current conditions, as well as cold water conditions (<1°C) (Steinsund et al., 1994; Polyak et al., 2002). The species introduction might be an indicator of either strong bottom currents occurring in front of the glacier terminus, or high influx of Arctic Water. The several high relative values of *E. excavatum* f. *clavata* may represent periods with lowering of the salinity, which can be an indicator of influx of Arctic water to the area, or runoff from the Waltershausen Gletscher.

As the high relative abundance of *S. loeblichi* found at 355 cm (5065 cal. yr. BP) coincides with a drop in the total foraminiferal flux, it is a possibility that due to high productivity over a period of time, the water mass has been depleted in oxygen, and the opportunistic species has moved into the area.

The total foraminiferal flux shows low values from the bottom of the zone up until the assemblage zone border at 185 cm (650 cal. yr. BP), where there is a sudden increase. The low values throughout the zone indicate unfavourable conditions, and limited food supply. If taking into account that dissolution of calcareous foraminifera happens at a much higher rate within water masses influenced by Polar water than Atlantic water (see *Chapter 5.1.1*), this could be an explanation for the low foraminiferal flux throughout the zone. However, as there were no clear signs of dissolution of the calcareous foraminifera, and the calculations of the foraminiferal flux are not reliable, this assumption is not so credible without any more evidence.

5.1.4 Assemblage zone 1

The fluctuating relative abundance of *C. reniforme,* and *E. excavatum* f. *clavata* could indicate an environment influenced with variations in inflow of Arctic water to the area, or a glacier-proximal environment. Both species may indicate a glacier-proximal environment, with the relative abundance of *E. excavatum* f. *clavata* often being higher closer to the glacier terminus (Korsun and Hald, 1998). High relative abundance of *E. excavatum* f. *clavata* indicates an environment with cold (<1°C) and low saline (30 – 34 ‰) bottom water. The high relative abundance of the opportunistic species is also related to increased glacial activity, high sedimentation rates and the presence of sea ice (Steinsund et al., 1994; Hald and Korsun, 1997; Jennings et al., 2004). According to Korsun and Hald, (1998), a foraminiferal assemblage dominated only by these two species alone, is not enough to determine a glacier-proximal environment. The relative abundance of *Q. stalkeri* increases from the lowest part of the zone towards the top. As this species is considered to possibly be an indicator of near-glacial, shallow marine habitats (Korsun and Hald, 1998), it is likely to believe that when relative high values of this species coincide with relative high values of *C. reniforme* and *E. excavatum* f. *clavata*, as it does at certain depths within AZ1, the environment is glacier-proximal. However, as the research on *Q. stalkeri* is limited, one cannot solely rely on the theory that the environment is glacier-proximal when high values of these three species coincide. Both *C. reniforme* and *E. excavatum* f. *clavata* are however found in more glacier-distal environments as well, and as the location of the core is situated approximately 11 km from the present glacier terminus, the fluctuations in the abundance are more likely to be caused by the presence of cold water masses. An explanation for the high abundance of *E. excavatum* f. *clavata* is lowering of the salinity within the area. This lowering could be caused by influx of low-saline Arctic Water, or terrestrial runoff.

The fact that both *A. gallowayi* and *C. lobatulus*, which are species thriving in high energy environments, have a low relative abundance might indicate that the energy conditions are lower within AZ 1, than AZ 2.

Three relative high values in the total foraminiferal flux are observed at 85 cm (243 cal. yr. BP), 65 cm (161 cal. yr. BP), and 35 cm (39 cal. yr. BP). It is also worth mentioning that the highest total foraminiferal flux values coincide with relatively low values of *E. excavatum* f. *clavata*, indicating that the environment has been more favourable for other species at these levels. More favourable conditions could be caused by influx of more saline water masses.

5.2 Paleoceanographic and paleoclimatic development during Holocene

In the following subchapters the results discussed above will be presented and tried to explain in context with the main time periods during the mid-late Holocene, comprising the Holocene Climate Optimum, the Neoglaciation, and the last 2000 cal. yr. BP. Reconstruction of the paleoceanography and paleoclimate is based on the results from the foraminiferal analysis, combined with results found from Olsen (2015), concerning the sedimentary paleoenvironment.

As the dating from the lowermost level of core HH13-012GC-TUNU has an age of 7771 cal. yr. BP, the core covers the Holocene Climate Optimum (>8000 – 4500 cal. yr. BP), the Neoglaciation and Medieval Warm Period (~4500 – 800 cal. yr. BP), the Little Ice Age (~800 – 100 cal. yr. BP), and the Modern Maximum (~100 cal. yr. BP - present) (Figure 10 and Figure 11). The onset of the main time periods are established based on previous studies of the paleoclimate of the area (see *Chapter 1.3.2* Holocene paleoclimate development)

As seen from Figure 10 and Figure 11, there is a slight offset between the borders in the established assemblage zones, and the onset of the Neoglaciation and the Little Ice Age. One reason for this might be that the age model (Figure 6) used for the boundaries assumes a constant sedimentation rate between the two dated levels, and does not take the assumed turbidites into account, which might indicate hiatus. Both the estimated onset of the Neoglaciation and the Little Ice Age lie within this area, and therefore one cannot rely solely on the estimated depths of the dates. Another possible explanation for the offset between the assemblage zone borders, and the time period divisions is that the onset of the different climatic periods varies regionally. This will be discussed further in the following subchapters.

5.2.1 Onset of climatic periods during the late Holocene in Nordfjord

As mentioned above, the dating of the different time periods in Figure 10 and Figure 11 are based on previous climatic research from the area. By comparing the results found in this study to other research, and assuming the age model is reliable, some of the borders can be readjusted (Figure 12). The suggested onset of the Neoglaciation is adjusted from 4500 cal. yr. BP to 5200 cal. yr. BP, and the onset of the Little Ice Age is adjusted from 800 cal. yr. BP to 600 cal. yr. BP. The age and depth of the different periods can be seen from Table 4.

Table 4: Age and depth of the different climatic periods within the Late Holocene, found from core HH13-012GC-TUNU.

Climatic Period	Depth (cm)	Age (cal. yr. BP)
Holocene Climate Optimum	454 – 360	>7771 – 5200
Neoglaciation	360 – 180	~ 5200 – 600
The Little Ice Age	180 – 35	~ 600 – 50
Modern Maximum	35 – 0	~ 50 – present

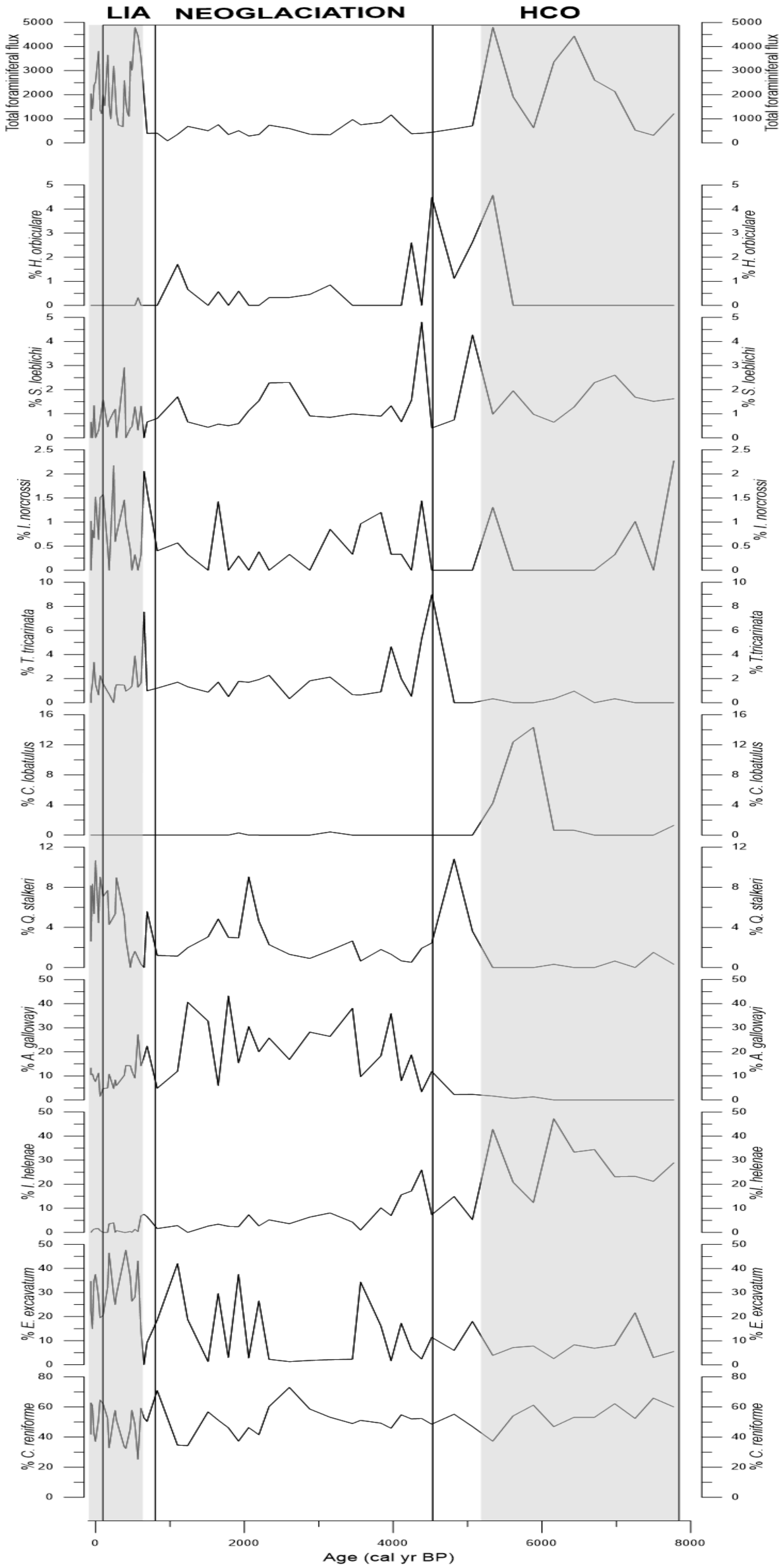

Figure 10: Core HH13-012GC-TUNU divided into time periods through the Holocene, established by previous studies of the paleoclimate of the area (HCO – Holocene Climate Optimum, Neoglaciation, and LIA – the Little Ice Age). Percentage abundance of the most common species found within the core is plotted against age. The established foraminiferal assemblage zones AZ 1-AZ 3 are indicated by the shaded grey areas.

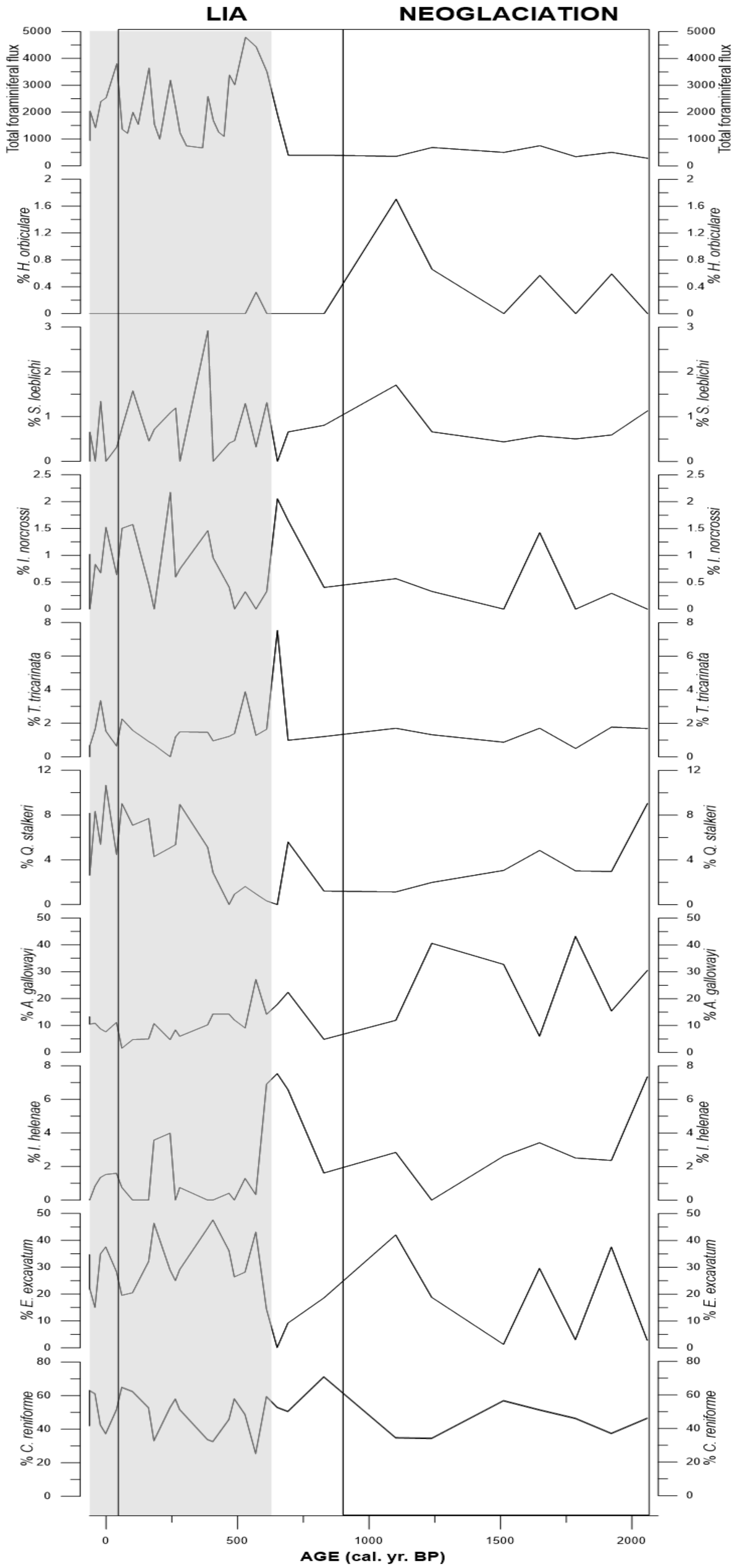

Figure 11: Core HH13-012GC-TUNU divided into time periods through the last 2000 cal. yr. BP, established by previous studies of the paleoclimate of the area (Neoglaciation, and LIA – the Little Ice Age). Percentage abundance of the most common species found within the core is plotted against age. The established foraminiferal assemblage zone AZ 1 is indicated by shaded grey area.

5.2.2 Holocene Climate Optimum (>7771 – 5200 cal. yr. BP)

The Holocene Climate Optimum covers the depth from ~454 – 335 cm within the core. As seen from Figure 10, the section between these two levels is located within AZ3, and the lowermost part of AZ2. However, the established termination of the Holocene Climate Optimum, and onset of the Neoglaciation, are positioned 25 cm from the border to AZ2, which from the age model constitutes ~700 years.

As mentioned in chapter 1.3.2, the Holocene Climate Optimum was a period with warm and dry summers, combined with high summer insolation. The date of termination for this period is however, varying regionally. Simpson et al., (2009) found in their study, reconstructing the extent of the Greenland Ice Sheet (GIS) from the Last Glacial Maximum to present-day, that between 5 – 4 ka BP the ice margin retreated approximately 80 km behind its present day position in the northeast of Greenland. On the other hand, records from lake sediments, retrieved from Geographical Society Ø near Kaiser Franz Josephs Fjord, indicate that a period with high precipitation rates and increase in snow accumulation commenced at ~6500 cal. yr. BP, followed by a decrease in the temperature around 5000 cal. yr. BP (Wagner et al., 2000). Olsen, (2015) found from her research that this cooling could have caused the Waltershausen Gletscher to advance into tidewater.

From the benthic calcareous foraminifera found within this timespan, the strong presence of *C. reniforme* combined with the high relative abundance of *I. helenae* indicate the environment is glacier-distal from the bottom of the core up until ~ 6000 cal. yr. BP. The two species combined with the high foraminiferal flux, give an indication of that seasonal sea-ice influenced the area, as seasonal sea ice enhances primary production (Ribeiro et al., 2017). Due to the high foraminiferal flux and the species found within this time span, it can be assumed that the influence of Polar water to the area has been low, and warmer Atlantic water has occupied the sea floor.

The high relative abundance of *C. lobatulus* from ~ 6000 – 5475 cal. yr. BP indicates a period of high energy. This could be a result of the increased precipitation rate in the area during this period, leading to terrestrial runoff causing turbulence. However, as *C. lobatulus* is found within water masses with relatively high salinity, the reason might instead be a strong inflow of recirculated Atlantic Water from the EGC, or a combination of both.

Perner et al., (2015) found from their paleoceanographic research based on planktic and benthic foraminifera assemblage data, on the shelf east of Kaiser Franz Josef Fjord, that relatively warm subsurface water influenced the Eastern Greenland shelf until ~ 4.5 ka BP. Their results coincide with the results found from the Greenland Sea, where Telesiński et al., (2014a) also claim that the influence of warm subsurface waters was amplified during this time span.

From 5338 cal. yr. BP (365 cm) the general decrease of both *I. helenae* and the total foraminiferal flux, combined with the occurrence of species as *E. excavatum* f. *clavata* and *Q. stalkeri*, indicate that the environment changed, with influence of more Arctic water. This faunal change corresponds well with the alleged decrease in temperature ~5000 cal. yr. BP found from the Geographical Society Ø, and the theory that the cooling climate led to Waltershausen Gletscher turning into tidewater presented by Olsen (2015).

These findings imply that the termination of the Holocene Climate Optimum is found at 360 cm, and not 335 cm which was established by dates from previous research from the area. This discrepancy constitutes ~700 years, and would, assuming the age model is correct, shift the date of termination of Holocene Climate Optimum to ~5200 cal. yr. BP. By shifting the date of termination, the border between the Holocene Climate Optimum and the Neoglaciation coincides with the border between AZ3 and AZ2 (Figure 12).

5.2.3 Neoglaciation (~ 5200 – 2000 cal. yr. BP)

In Figure 10 the Neoglaciation and Medieval Warm period cover the depth from 335 – 200 cm. However, as the termination of the Holocene Climate Optimum should coincide with the onset of the Neoglaciation, the lower limit should be at 5200 cal. yr. BP.

The high precipitation rates continued until ~3000 cal. yr. BP, whereas the climatic cooling lasted until ~1000 cal. yr. BP, which culminated in the last 2000 years of the period consisting of a cold and dry climate (Wagner et al., 2000). The onset of the Neoglacial cooling came as a result of a decrease in insolation, commencing at 7 ka. BP, which was enhanced by inflow of cold Polar Water in the Nordic Seas (Telesiński et al., 2014a). Due to the Neoglaciation, glaciers expanded all over Greenland(Bennike and Weidick, 2001). The initiation time of the glacier expansion did, on the other hand, vary largely. Expansion started in northeast Greenland at ~5000 year BP (Hjort, 1997), whereas studies from Scoresby Sund, south of Kaiser Franz Josephs Fjord, indicate that the expansion started approximately 2000 years later than in the northeast (Funder et al., 1989).

The general decrease in *I. helenae*, combined with the occurrence of cold water species as *E. excavatum* f. *clavata* and *A. gallowayi*, are clear indicators of that the area is more influenced by arctic water from ~ 5200 cal. yr. BP. This theory coincides well with findings from the North Iceland shelf based on drift ice, and sea surface temperatures, which indicate an increase in Artic water influence after ~5.5 ka BP (Moros et al., 2006).

In the beginning of the Neoglaciation *A. gallowayi* is introduced. The species thrives in cold waters with high energy conditions, and as there is a change in the environment from the Holocene Climate Optimum to the Neoglaciation, it is reasonable to assume that higher energy conditions occurred in the area. Several levels with high relative abundance of *E. excavatum* f. *clavata* in the uppermost part of the core covering the Neoglaciation indicate periods with higher inflow of low saline polar water.

Findings from the eastern Greenland shelf indicate a southwards movement of the polar front and perennial sea ice (Perner et al., 2015). This would likely have made Nordfjord ice covered year round. A constant sea ice cover, combined with the cold water masses occupying the fjord, could be an explanation for the low total foraminiferal flux throughout the entire Neoglaciation.

5.2.4 Last 2000 cal. yr. BP

As seen from Figure 11, the last 2000 cal. yr. BP cover the youngest period of Neoglaciation, which includes the Medieval Warm Period, the Little Ice Age, and the Modern Maximum, which is the present climate warming.

5.2.4.1 Medieval Warm Period

During the end of the Neoglaciation, the Medieval Warm Period (MWP), which is suggested to have commenced at ~1000 cal. yr. BP, and lasted for approximately 200 years, occurred (Wagner et al., 2000). From Nansen Fjord in south-eastern Greenland, Jennings and Weiner, (1996) identified the MWP as a period with relatively warm and stable climate lasting from 730 – 1110 cal. AD, where Atlantic Intermediate Water dominated the seabed within the fjord. This is suggested to be a result of relatively low influx of Polar Water, or strong influx of Atlantic Water. Miettinen et al., (2015) found from a diatom analysis from a core recovered from Kangerlussuaq Trough on the SE Greenland shelf, that from ~1000 C.E, an abrupt warming occurred, increasing the sea surface temperature with ~2.4℃ in only ~55 years. The warm period lasted until ~1200 C.E, and is seen as the local signal of the MWP. From their study on the Eastern Greenland shelf, Perner et al., (2015), observed a minor increase in agglutinated species thriving in Atlantic Intermediate Water at ~1.0 ka BP, indicating an increase in chilled Atlantic Water influencing the area.

In this study there is no clear evidence of the climatic event affecting the area. However, as there are only two samples from within the time span covering MWP, one cannot determine this statement with certainty from the results provided from the analysis of the calcareous benthic foraminifera found within HH13-012GC-TUNU alone. Wagner et al., (2000) did during their research on pollen within Keiser Franz Josephs Fjord, identify a period of warming lasting from ~900 – 500 cal. yr. BP.

5.2.4.2 The Little Ice Age (~ 600 – 50 cal. yr. BP)

By the previous climatic research in the area, The Little Ice Age commences ~800 cal. yr. BP (200 cm), and as seen from Figure 10 and Figure 11 there is an offset between the onset of The Little Ice Age and the start of AZ 1 of 20 cm. As the dominance of *E. excavatum* f. *clavata* does not start until 630 cal. yr. BP, combined with the end of the warm period identified by Wagner et al., (2000), it is not unlikely that this marks the onset of the Little Ice Age within the area. The onset of the period thereby coincides with the onset of AZ 1.

The Little Ice Age was the coldest period within the Holocene, and precipitation rates increased slightly from the Medieval Warm period (Wagner et al., 2000). The conditions would suggest glacier expansion, and glaciers in Norway and Svalbard did advance during the Little Ice Age. However, during her research, Olsen (2015), did not find any clear evidence that the core location had been overridden by the glacier, indicating that a potential glacier advance must have been less than 10 km from the present day glacier terminus.

The dominance of the cold water species *E. excavatum* f. *clavata* occurs at ~630 cal. yr. BP, which coincides roughly with the end of the warmer period identified by Wagner et at., (2000). Following this level, the dominance of *E. excavatum* f. *clavata* and *C. reniforme* indicate an environment influenced by Arctic water.

In addition, the total foraminiferal flux also fluctuates through the period. Olsen (2015) discovered that a change in turbidites found within the core towards the end of Little Ice Age, could be indicative of warm intervals intervening the otherwise cold and harsh time period. As there are found several intervals of decreased values in the relative abundance of *E. excavatum* f. *clavata* that coincide with high relative values in the total foraminiferal flux, these fluctuations in the climate are not inconceivable. In addition, Perner et al., (2015) suggest that from ~1.4 ka BP, sea ice conditions in Fosters Bugt, at the mouth of Kaiser Franz Josephs Fjord, went back to seasonal cover, which would enhance primary production, and thereby more favourable conditions.

5.2.4.3 Modern Maximum (50 cal. yr. BP – present)

The Modern Maximum is the present warming period, and commenced at the termination of the Little Ice Age. The temperatures started increasing, before a cold period from the 1970s to early 1990s AD, followed by a new warming reaching the present day temperature (Kobashi et al., 2015).

From the sedimentological study by Olsen (2015), an increased amount of sand found within the top of the core, could imply an increased meltwater discharge from the Waltershausen Gletscher following the termination of the Little Ice Age. The author is however, uncertain whether the glacier has retreated or not.

The foraminiferal fauna shows little variation from the Little Ice Age and into the Modern Maximum, and the depth of where the Little Ice Age terminates and the Modern Maximum commence is therefore hard to determine. There is no clear evidence of warming of the water masses, which would suggest that Arctic Water still has a strong influence in the area. A study from the North Icelandic shelf, based on benthic and planktonic foraminiferal assemblages, stable isotope values, and ice rafted debris concentrations, shows the same results, with no signs of water masses warming during the last decades (Knudsen et al., 2004)

However, in this study there are only five foraminiferal samples from the last decade, and only three samples from after the warming in the 1990s, and one can therefore not conclude that the present climatic warming does not affect the area.

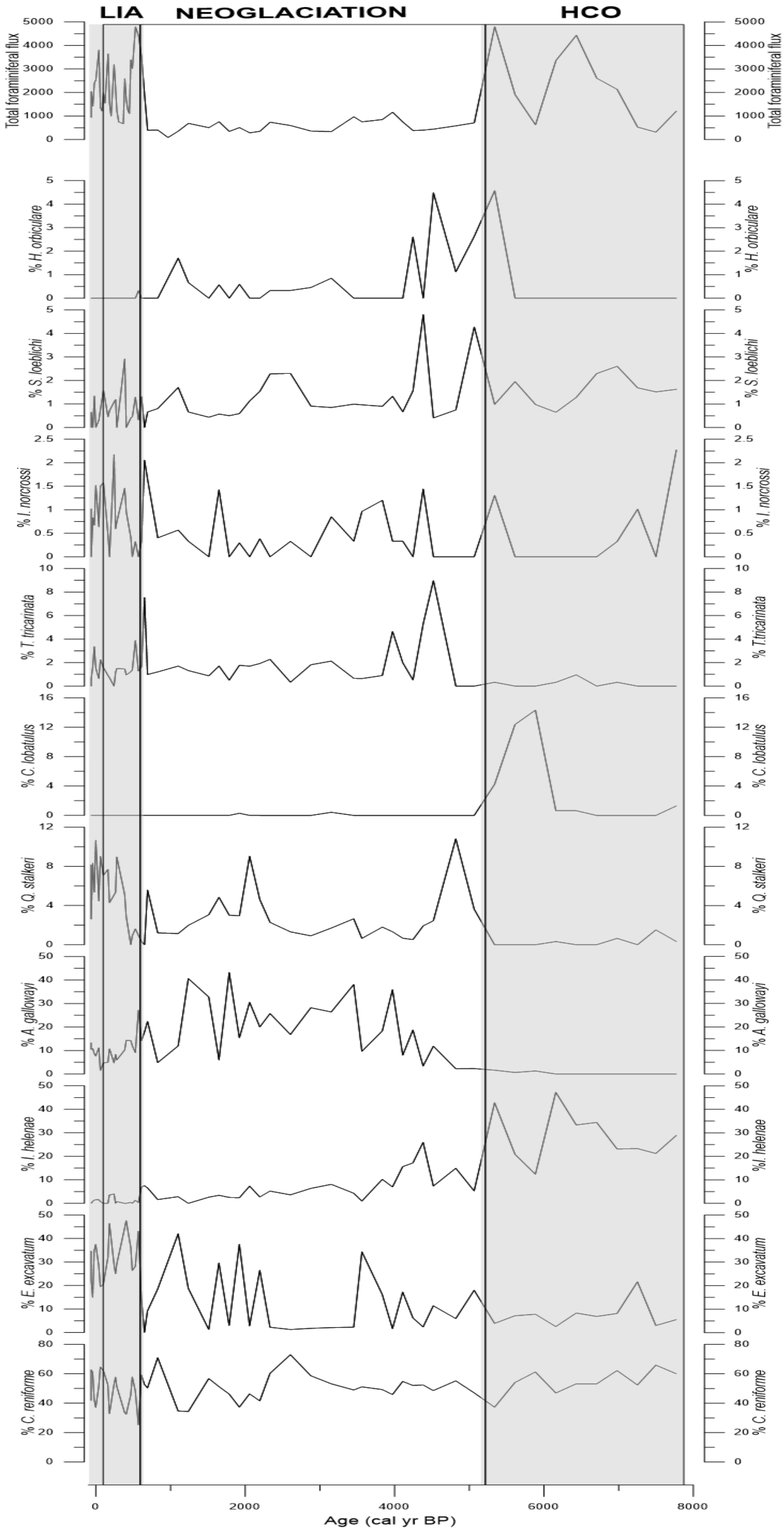

Figure 12: Percentage abundance of the calcareous benthic foraminifera found within Core HH13-012GC-TUNU, seen with regards to the different climatic periods within the late Holocene. (HCO - Holocene Climate Optimum, the Neoglaciation, and LIA – the Little Ice Age)

6. Conclusions

The study of benthic foraminifera from core HH13-012GC-TUNU shows the paleoceanographic development within Nordfjord, North-East Greenland, during the mid- and late Holocene. The main outcomes from this study are as follows:

- The strong presence of *C. reniforme* throughout the entire core is an indicator of that the conditions within Nordfjord have been that of a glaciomarine environment during the last ~7800 cal. yr. BP.
- Based on the benthic calcareous foraminiferal fauna, the core was divided into three assemblage zones. Each of the assemblage zones coincides with the main climatic periods in the mid- to late Holocene, which are the Holocene Climate Optimum, the Neoglaciation, and the Little Ice Age.
- The Holocene Climate Optimum lasted from >7770 – 5200 cal. yr. BP. The foraminiferal fauna within the period is dominated by *Cassidulina reniforme* and *Islandiella Helenae*, indicating inflow of recirculated Atlantic Water from the Eastern Greenland Current, and seasonal sea ice conditions.
- During the Neoglaciation, the area was within the Polar Front, and the perennial sea ice covered the area. The introduction of the cold water species *Astrononion Gallowayi* and *Elphidium Excavatum* f. *clavata* indicates a transition from inflow of Atlantic Water to inflow of Arctic Water to the fjord from ~5200 cal. yr. BP in addition to an increase in the energy at the sea floor.
- The onset of the Little Ice Age is defined by an abrupt increase in relative abundance of *Elphidium Excavatum* f. *clavata*, at ~630 cal. yr. BP. The composition of the foraminiferal fauna within the period indicates continued inflow of Arctic Water. In addition, a northwards movement of the Polar Front gives seasonal sea ice conditions, and enhanced primary production.
- The onset of the Modern Maximum is hard to determine from the results, as there is no clear boundary to the termination of The Little Ice Age. This indicates that the water masses influencing the fjord, have not changed remarkably the last 100 years, and that Arctic Water is still occupying seafloor.

References

Aagaard, K., Coachman, L.K., 1968. The East Greenland Current North of Denmark Strait: Part I. *Arctic 21*, 181–200.

Allaby, M., 2013. Dictionary of Plant Sciences [WWW Document]. Oxf. Ref. URL http://www.oxfordreference.com/view/10.1093/acref/9780199600571.001.0001/acref-9780199600571 (accessed 11.27.16).

Alley, R.B., Andrews, J.T., Brigham-Grette, J., Clarke, G.K.C., Cuffey, K.M., Fitzpatrick, J.J., Funder, S., Marshall, S.J., Miller, G.H., Mitrovica, J.X., Muhs, D.R., Otto-Bliesner, B.L., Polyak, L., White, J.W.C., 2010. History of the Greenland Ice Sheet: paleoclimatic insights. *Quat. Sci. Rev., Special Theme: Arctic Palaeoclimate Synthesis* (PP. 1674-1790) 29, 1728–1756.

Andrews, J.T., Jennings, A.E., 2014. Multidecadal to millennial marine climate oscillations across the Denmark Strait (~ 66 ºN) over the last 2000 cal yr. BP. *Clim. Past 10*, 325–343.

Azetsu-Scott, K., Tan, F.C., 1997. Oxygen isotope studies from Iceland to an East Greenland Fjord: behaviour of glacial meltwater plume. *Mar. Chem. 56*, 239–251.

Barber, D.C., Dyke, A., Hillaire-Marcel, C., Jennings, A.E., Andrews, J.T., Kerwin, M.W., Bilodeau, G., McNeely, R., Southon, J., Morehead, M.D., Gagnon, J.-M., 1999. Forcing of the cold event of 8,200 years ago by catastrophic drainage of Laurentide lakes. *Nature 400*, 344–348.

Bennike, O., Weidick, A., 2001. Late Quaternary history around Nioghalvfjerdsfjorden and Jøkelbugten, North-East Greenland. *Boreas 30*, 205–227.

Bradley, R.S., 2015. Chapter 6 - Marine Sediments, in: Paleoclimatology (Third Edition). Academic Press, San Diego, pp. 195–277.

Cottier, F.R., Nilsen, F., Skogseth, R., Tverberg, V., Skarðhamar, J., Svendsen, H., 2010. Arctic fjords: a review of the oceanographic environment and dominant physical processes. *Geol. Soc. Lond. Spec. Publ. 344*, 35–50.

Dias, B.B., Hart, M.B., Smart, C.W., Hall-Spencer, J.M., 2010. Modern seawater acidification: the response of foraminifera to high-CO2 conditions in the Mediterranean Sea. *J. Geol. Soc. 167*, 843–846.

Evans, J., Dowdeswell, J.A., Grobe, H., Niessen, F., Stein, R., Hubberten, H.-W., Whittington, R., 2002. Late Quaternary sedimentation in Kejser Franz Joseph Fjord and the continental margin of East Greenland. *Geol. Soc. Lond. Spec. Publ. 203*, 149–179.

Farmer, D.M., Freeland, H.J., 1983. The physical oceanography of Fjords. *Prog. Oceanogr. 12*, 147–219.

Feyling-Hanssen, R.W., 1964. Foraminifera in late Quaternary deposits from the Oslofjord area. Universitetsforlaget, Oslo.

Funder, S., Larsen, H.C., Fredskild, B., 1989. Quaternary geology of the ice-free areas and adjacent shelves of Greenland, in: Quarternary Geology of Canada and Greenland, R.J. Fulton. Geological Survey of Canada, Canada, pp. 741–792.

Haakansson, S., 1973. University of Lund radiocarbon dates VI. *Radiocarbon 15*, 493–513.

Hald, M., Korsun, S., 1997. Distribution of modern benthic foraminifera from fjords of Svalbard, European Arctic. *J. Foraminifer. Res. 27*, 101–122.

Hald, M., Steinsund, P.I., 1992. Distribution of surface sediment benthic Foraminifera in the southwestern Barents Sea. *J. Foraminifer. Res. 22*, 347–362.

Hambrey, M.J., 1994. Glacial Environments. UBC Press.

Hansen, A., Knudsen, K.L., 1995. Recent foraminiferal distribution in Freemansundet and Early Holocene stratigraphy on Edgeøya, Svalbard. *Polar Res. 14*, 215–238.

Hermelin, J.O.R., Scott, D.B., 1985. Recent Benthic Foraminifera from the Central North Atlantic. *Micropaleontology 31*, 199–220.

Hjort, C., 1997. Glaciation, climate history, changing marine levels and the evolution of the Northeast Water polynya. *J. Mar. Syst. 10*, 23–33.

Hubberten, H.-W., 1995. Die Expedition ARKTIS-X/2 mit FS “Polarstern” 1994 = The expedition ARKTIS-X/2 of RV “Polarstern” in 1994. MyScienceWork.

Husum, K., Hald, M., 2004. Modern Foraminiferal Distribution in the Subarctic Malangen Fjord and Adjoining Shelf, Northern Norway. *J. Foraminifer. Res. 34*, 34–48.

Ivanova, E.V., Ovsepyan, E.A., Risebrobakken, B., Vetrov, A.A., 2008. Downcore Distribution of Living Calcareous Foraminifera and Stable Isotopes in the Western Barents Sea. *J. Foraminifer. Res. 38*, 337–356.

Jennings, A.E., Helgadottir, G., 1994. Foraminiferal assemblages from the fjords and shelf of eastern Greenland. *J. Foraminifer. Res. 24*, 123–144.

Jennings, A.E., Weiner, N.J., 1996. Environmental change in eastern Greenland during the last 1300 years: Evidence from foraminifera and lithofacies in Nansen Fjord, 68°N. *ResearchGate 6*, 179–191.

Jennings, A.E., Weiner, N.J., Helgadottir, G., Andrews, J.T., 2004. Modern Foraminiferal Faunas of the Southwestern to Northern Iceland Shelf: Oceanographic and Environmental Controls. *J. Foraminifer. Res. 34*, 180–207.

Knudsen, K.L., Eiríksson, J., Jansen, E., Jiang, H., Rytter, F., Ruth Gudmundsdóttir, E., 2004. Palaeoceanographic changes off North Iceland through the last 1200 years: foraminifera, stable isotopes, diatoms and ice rafted debris. *Quat. Sci. Rev., Holocene climate variability - a marine perspective 23*, 2231–2246.

Kobashi, T., Box, J.E., Vinther, B.M., Goto-Azuma, K., Blunier, T., White, J.W.C., Nakaegawa, T., Andresen, C.S., 2015. Modern solar maximum forced late twentieth century Greenland cooling. *Geophys. Res. Lett. 42*, 5992-5999.

Korsun, S., Hald, M., 1998. Modern Benthic Foraminifera off Novaya Zemlya Tidewater Glaciers, Russian Arctic. *Arct. Alp. Res. 30*, 61–77.

Kubischta, F., Knudsen, K.L., Kaakinen, A., Salonen, V.-P., 2010. Late Quaternary foraminiferal record in Murchisonfjorden, Nordaustlandet, Svalbard. *Polar Res. 29*, 283–297.

Linke, P., Lutze, G.F., 1993. Microhabitat preferences of benthic foraminifera—a static concept or a dynamic adaptation to optimize food acquisition? *Mar. Micropaleontol. 20*, 215–234.

Lloyd, J.M., 2006. Late Holocene environmental change in Disko Bugt, west Greenland: interaction between climate, ocean circulation and Jakobshavn Isbrae. *Boreas 35*, 35–49.

Lloyd, J.M., Park, L.A., Kuijpers, A., Moros, M., 2005. Early Holocene palaeoceanography and deglacial chronology of Disko Bugt, West Greenland. *Quat. Sci. Rev. 24*, 1741–1755.

Mangerud, J., 1972. Radiocarbon dating of marine shells, including a discussion of apparent age of Recent shells from Norway. *Boreas 1*, 143–172.

Mann, M.E., Zhang, Z., Rutherford, S., Bradley, R.S., Hughes, M.K., Shindell, D., Ammann, C., Faluvegi, G., Ni, F., 2009. Global Signatures and Dynamical Origins of the Little Ice Age and Medieval Climate Anomaly. *Science 326*, 1256–1260.

Marshall, J., Schott, F., 1999. Open-ocean convection: Observations, theory, and models. *Rev. Geophys. 37*, 1–64.

Miettinen, A., Divine, D.V., Husum, K., Koç, N., Jennings, A., 2015. Exceptional ocean surface conditions on the SE Greenland shelf during the Medieval Climate Anomaly. *Paleoceanography 30*, 1657-1674.

Moros, M., Andrews, J.T., Eberl, D.D., Jansen, E., 2006. Holocene history of drift ice in the northern North Atlantic: Evidence for different spatial and temporal modes. *Paleoceanography 21*, PA2017.

Olsen, I.L., 2015. Sedimentary processes and paleoenvironments in Moskusoksefjord and Nordfjord, North-East Greenland.

Perner, K., Moros, M., Lloyd, J.M., Jansen, E., Stein, R., 2015. Mid to late Holocene strengthening of the East Greenland Current linked to warm subsurface Atlantic water. *Quat. Sci. Rev. 129*, 296–307.

Polyak, L., Korsun, S., Febo, L.A., Stanovoy, V., Khusid, T., Hald, M., Paulsen, B.E., Lubinski, D.J., 2002. Benthic Foraminiferal Assemblages from the Southern Kara Sea, a River-Influenced Arctic Marine Environment. *J. Foraminifer. Res. 32*, 252–273.

Rahmstorf, S., 1995. Bifurcations of the Atlantic thermohaline circulation in response to changes in the hydrological cycle. *Nature 378*, 145–149.

Reimer, P.J., Bard, E., Bayliss, A., Beck, J.W., Blackwell, P.G., Bronk Ramsey, C., Buck, C.E., Cheng, H., Edwards, R.L., Friedrich, M., Grootes, P.M., Guilderson, T.P., Haflidason, H., Hajdas, I., Hatté, C., Heaton, T.J., Hoffmann, D.L., Hogg, A.G., Hughen, K.A., Kaiser, K.F., Kromer, B., Manning, S.W., Niu, M., Reimer, R.W., Richards, D.A., Scott, E.M., Southon, J.R., Staff, R.A., Turney, C.S.M., van der Plicht, J., 2013a. IntCal13 and Marine13 radiocarbon age calibration curves 0-50,000 years cal BP 55, 1869–1887.

Reimer, P.J., Reimer, R.W., Blaauw, M., 2013b. RADIOCARBON DATING | Calibration of the 14C Record, in: Elias, S.A., Mock, C.J. (Eds.), *Encyclopedia of Quaternary Science (Second Edition)*. Elsevier, Amsterdam, pp. 345–352.

Ribeiro, S., Sejr, M.K., Limoges, A., Heikkilä, M., Andersen, T.J., Tallberg, P., Weckström, K., Husum, K., Forwick, M., Dalsgaard, T., Massé, G., Seidenkrantz, M.-S., Rysgaard, S., 2017. Sea ice and primary production proxies in surface sediments from a High Arctic Greenland fjord: Spatial distribution and implications for palaeoenvironmental studies. *Ambio 46*, 106–118.

Seidenkrantz, M.-S., 2013. Benthic foraminifera as palaeo sea-ice indicators in the subarctic realm – examples from the Labrador Sea–Baffin Bay region. *Quat. Sci. Rev. 79*, 135–144.

Shindell, D.T., Schmidt, G.A., Miller, R.L., Mann, M.E., 2003. Volcanic and Solar Forcing of Climate Change during the Preindustrial Era. *J. Clim. Boston 16*, 4094–4107.

Simpson, M.J.R., Milne, G.A., Huybrechts, P., Long, A.J., 2009. Calibrating a glaciological model of the Greenland ice sheet from the Last Glacial Maximum to present-day using field observations of relative sea level and ice extent. *Quat. Sci. Rev. 28*, 1631–1657.

Steinsund, P.I., Polyak, L., Hald, M., Mikhailov, V., Korsun, S., 1994. Distribution of calcareous benthic foraminifera in recent sediments of the Barents and Kara Seas.

Stigebrandt, A., 1976. Vertical Diffusion Driven by Internal Waves in a Sill Fjord. *J. Phys. Oceanogr. 6*, 486–495.

Stuiver, M., Braziunas, T.F., 1993. Modeling atmospheric (super 14) C influences and (super 14) C ages of marine samples to 10,000 BC. *Radiocarbon 35*, 137–189.

Syvitski, J.P.M., Burrell, D.C., Skei, J.M., 1987. Fjords: Processes and Products. Springer Science & Business Media.

Telesiński, M.M., Spielhagen, R.F., Bauch, H.A., 2014b. Water mass evolution of the Greenland Sea since late glacial times. *Clim Past 10*, 123–136.

Telesiński, M.M., Spielhagen, R.F., Lind, E.M., 2014a. A high-resolution Lateglacial and Holocene palaeoceanographic record from the Greenland Sea. *Boreas 43*, 273–285.

Wagner, B., Melles, M., Hahne, J., Niessen, F., Hubberten, H.-W., 2000. Holocene climate history of Geographical Society Ø, East Greenland — evidence from lake sediments. *Palaeogeogr. Palaeoclimatol. Palaeoecol. 160*, 45–68.

Wang, P., Chappell, J., 2001. Foraminifera as Holocene environmental indicators in the South Alligator River, Northern Australia. *Quat. Int. 83–85*, 47–62.

Watts, A., 2010. Greenland glaciers – melt due to sea current change, not air temperature [WWW Document]. Watts That. URL https://wattsupwiththat.com/2010/02/16/greenland-glaciers-melt-due-to-sea-current-change-not-air-temperature/ (accessed 11.10.16).

Wollenburg, J.E., Mackensen, A., 1998. Living benthic foraminifers from the central Arctic Ocean: faunal composition, standing stock and diversity. *Mar. Micropaleontol. 34*, 153–185.

Appendix

Appendix 1 – Depth-Age estimations

This appendix contains the assumed ages of each sample within core HH13-012GC-TUNU. The middle column represents the ages used in this study, and the right column represents the ages of an assumed linear sedimentation rate.

Depth (cm)	Age (Cal yr. BP) – change in sedimentation rate	Age (Cal yr. BP) - assumed linear sedimentation rate
454	7771	7771
450	7662	7662
444	7498	7498
440	7388	7388
435	7252	7252
430	7115	7115
425	6978	6978
420	6842	6842
415	6705	6705
410	6568	6568
405	6432	6432
400	6295	6295
395	6158	6158
390	6022	6022
385	5885	5885
380	5748	5748
375	5612	5612
370	5475	5475
365	5338	5338
361	5229	5229
355	5065	5065
350	4928	4928
346	4819	4819
340	4655	4655
335	4518	4518
330	4381	4381
325	4245	4245
320	4108	4108
315	3971	3971
310	3835	3835
305	3698	3698
300	3561	3561
296	3452	3452
290	3288	3288
285	3151	3151

280	3015	3015
275	2878	2878
270	2741	2741
265	2605	2605
260	2468	2468
255	2331	2331
250	2195	2195
245	2058	2058
240	1921	1921
235	1784	1784
230	1648	1648
225	1511	1511
220	1374	1374
215	1238	1238
210	1101	1101
205	964	964
200	828	828
195	691	691
185	650	418
180	630	281
175	609	144
170	589	8
165	569	-129
160	548	-266
155	528	-402
150	508	-539
145	487	-676
140	467	-812
135	446	-949
130	426	-1086
125	406	-1223
120	385	-1359
115	365	-1496
110	345	-1633
106	328	-1742
100	304	-1906
94	279	-2070
90	263	-2179
85	243	-2316
80	222	-2453
75	202	-2589
70	182	-2726
65	161	-2863
60	141	-2999

55	120	-3136
50	100	-3273
45	80	-3409
40	59	-3546
35	39	-3683
30	18	-3819
25	-2	-3956
20	-22	-4093
15	-43	-4229
10	-63	-4366
5	-63	-4503
0	-63	-4640

Appendix 2 – Number of calcareous, agglutinated and planktic species

In this appendix, the total number of calcareous, agglutinated, and planktic species found at the sampled depths are shown.

Depth (cm)	Age (cal. yr. BP)	Calcareous species	Agglutinated species	Planktic species
454	7771	308	0	19
444	7498	132	4	12
435	7252	296	0	14
425	6978	307	2	17
415	6705	305	0	18
405	6432	312	2	13
395	6158	309	1	15
385	5885	307	1	21
375	5612	307	0	28
365	5338	306	9	21
355	5065	304	17	34
346	4819	268	17	36
335	4518	245	30	0
330	4381	208	-	-
325	4245	192	8	0
320	4108	301	4	9
315	3971	301	13	22
310	3835	333	14	15
300	3561	311	17	13
296	3452	302	1	34
285	3151	235	4	17
275	2878	220	8	14
265	2605	304	7	17
255	2331	307	0	9
250	2195	260	0	9
245	2058	177	8	6
240	1921	338	5	8
235	1784	199	7	4
230	1648	351	21	3
225	1511	229	-	-
215	1238	303	0	10
210	1101	176	9	12
205	964	47	9	3
200	828	248	7	3
195	691	304	9	3
185	650	146	12	10
175	609	304	-	-

Depth (cm)	Age (cal. yr. BP)	Calcareous species	Agglutinated species	Planktic species
165	569	313	0	0
155	528	309	18	11
145	487	216	19	8
140	467	246	24	6
135	446	72	3	3
130	426	85	2	2
125	406	105	0	0
120	385	137	4	3
115	365	51	7	8
100	304	50	3	2
94	279	134	14	12
90	263	168	18	5
85	243	276	25	12
75	202	82	4	3
70	182	140	6	7
65	161	221	7	6
55	120	87	8	7
50	100	127	4	8
45	80	85	6	4
40	59	133	3	8
35	39	314	18	23
25	-2	197	12	6
20	-22	149	0	0
15	-43	120	11	4
10	-63	153	5	13
5	-63	70	7	3
0	-63	98	9	7

Appendix 3 – Number of foraminiferal specimens

This appendix contains two tables showing the counted number of each benthic calcareous foraminiferal species at every sampling depth within core HH13-012GC-TUNU.

Depth (cm)	Age (Cal yr. BP)	*C. reniforme*	*E. excavatum f. clavata*	*I. helenae*	*I. norcrossi*	*S. loeblichi*	*Q. stalkeri*	*A. gallowayi*	*C. lobatulus*	*T. tricarinata*	*H. orbiculare*	*M. barleeanus*	*P. lateralis*
454	7771	185	17	89	7	5	1	0	4	0	0	0	0
444	7498	87	4	27	0	2	2	0	0	0	0	1	4
435	7252	155	64	69	3	5	0	0	0	0	0	0	0
425	6978	191	25	71	1	8	2	0	0	1	0	5	0
415	6705	162	21	105	0	7	0	0	0	0	0	1	0
405	6432	166	26	104	0	4	0	0	2	3	0	5	0
395	6158	145	8	146	0	2	1	0	2	1	0	2	1
385	5885	188	24	38	0	3	0	4	44	0	0	2	2
375	5612	166	22	64	0	6	0	2	38	0	0	5	1
365	5338	114	12	131	4	3	0	5	13	1	14	6	1
355	5065	152	57	17	0	15	13	8	0	1	9	5	2
346	4819	149	16	40	0	2	29	6	0	0	4	2	0
340	4655	124	25	26	0	2	14	27	0	0	7	0	0
335	4518	119	28	18	0	1	6	29	0	22	11	2	2
330	4381	109	5	54	3	10	4	7	0	11	0	0	0
325	4245	100	12	33	0	3	1	36	0	1	5	0	0
320	4108	165	52	47	1	2	2	24	0	6	0	0	0

Depth (cm)	Age (Cal yr. BP)	*C. reniforme*	*E. excavatum f. clavata*	*I. helenae*	*I. norcrossi*	*S. loeblichi*	*Q. stalkeri*	*A. gallowayi*	*C. lobatulus*	*T. tricarinata*	*H. orbiculare*	*M. barleeanus*	*P. lateralis*
315	3971	138	5	21	1	4	4	108	0	14	0	0	0
310	3835	164	54	34	4	3	6	61	0	3	0	0	0
300	3561	159	107	3	3	3	2	30	0	2	0	1	0
296	3452	148	7	13	1	3	8	115	0	2	0	0	0
285	3151	125	5	19	2	2	4	62	1	5	2	1	0
280	3015	127	6	13	1	3	6	64	0	6	3	1	0
275	2878	129	4	14	0	2	2	62	0	4	1	0	0
265	2605	222	4	11	1	7	4	51	0	1	1	0	0
255	2331	185	7	16	0	2	7	79	0	7	1	0	0
250	2195	108	69	7	1	4	12	52	0	5	0	0	0
245	2058	82	5	13	0	2	16	54	0	3	0	0	0
240	1921	126	127	8	1	2	10	52	1	6	2	0	0
235	1784	92	6	5	0	1	6	86	0	1	0	0	0
230	1648	180	104	12	5	2	17	21	0	6	2	0	0
225	1511	130	3	6	0	1	7	75	0	2	0	0	0
215	1238	104	57	0	1	2	6	123	0	4	2	0	0
210	1101	61	74	5	1	3	2	21	0	3	3	0	0
205	964	32	2	1	2	0	4	3	0	1	0	0	0
200	828	176	46	4	1	2	3	12	0	3	0	0	0
195	691	153	28	20	5	2	17	68	0	3	0	0	0
185	650	77	11	11	3	0	0	26	0	11	0	1	0
175	609	180	44	21	1	4	1	43	0	5	0	0	0
165	569	79	135	1	0	1	3	85	0	4	1	0	0
155	528	150	87	4	1	4	5	28	0	12	0	0	0
145	487	125	57	0	0	1	2	26	0	3	0	1	0

Depth (cm)	Age (Cal yr. BP)	*C. reniforme*	*E. excavatum f. clavata*	*I. helenae*	*I. norcrossi*	*S. loeblichi*	*Q. stalkeri*	*A. gallowayi*	*C. lobatulus*	*T. tricarinata*	*H. orbiculare*	*M. barleeanus*	*P. lateralis*
140	467	112	89	1	1	1	0	35	0	3	0	0	0
135	446	37	19	0	1	0	1	13	0	1	0	0	0
130	426	48	26	3	0	2	3	3	0	0	0	0	0
125	406	34	50	0	1	0	3	15	0	1	0	1	0
120	385	46	61	0	2	4	7	14	0	2	0	0	0
115	365	27	17	1	0	1	3	0	0	1	0	0	0
110	345	24	18	1	1	1	4	2	0	1	0	0	0
106	328	25	15	2	1	0	8	4	0	0	0	0	0
100	304	26	14	1	0	0	6	3	0	0	0	0	0
94	279	69	39	1	1	0	12	8	0	2	0	0	0
90	263	97	42	0	1	2	9	14	0	2	0	0	0
85	243	145	80	11	6	3	14	13	0	0	0	1	0
80	222	41	22	1	0	2	6	14	0	0	0	0	0
75	202	39	18	1	0	3	7	14	0	0	0	0	0
70	182	46	65	5	0	1	6	15	0	1	0	0	0
65	161	116	71	0	1	1	17	11	0	2	0	1	0
60	141	36	18	0	0	0	14	17	0	0	0	0	0
55	120	38	16	0	0	0	15	15	0	1	0	0	0
50	100	79	26	0	2	2	9	6	0	2	0	0	0
45	80	59	11	0	2	0	3	8	0	2	0	0	0
40	59	86	26	1	2	1	12	2	0	3	0	0	0
35	39	161	89	5	2	1	14	35	0	2	0	0	0
25	-2	73	74	3	3	0	21	15	0	3	0	0	0
20	-22	63	52	2	1	2	8	13	0	5	0	0	0
15	-43	73	18	1	1	0	10	13	0	2	0	0	0

Depth (cm)	Age (Cal yr. BP)	*C. reniforme*	*E. excavatum f. clavata*	*I. helenae*	*I. norcrossi*	*S. loeblichi*	*Q. stalkeri*	*A. gallowayi*	*C. lobatulus*	*T. tricarinata*	*H. orbiculare*	*M. barleeanus*	*P. lateralis*
10	-63	96	34	0	0	1	4	16	0	1	0	0	0
5	-63	23	35	0	0	0	5	7	0	0	0	0	0
0	-63	41	34	0	1	0	8	13	0	0	0	0	0

Depth (cm)	Age (Cal. yr. BP)	*S. fusiformis*	*E. hallandense*	*S. groenlandica*	*F. laevigata*	*C. teretis*	*C. laevigata*	*T. trihedra*	*D. Trondheimensis*	*Globobulimina Sp.*	*D. drammenensis*	*L. clavata*	*L. linearis*
454	7771	0	0	0	0	0	0	0	0	0	0	0	0
444	7498	0	0	0	0	0	0	0	0	0	0	0	0
435	7252	0	0	0	0	0	0	0	0	0	0	0	0
425	6978	1	0	0	0	0	0	0	0	0	0	0	0
415	6705	0	1	0	0	0	0	0	0	0	0	0	0
405	6432	0	0	1	0	0	0	0	0	0	0	0	0
395	6158	0	0	0	0	0	0	0	0	0	0	0	0
385	5885	1	1	0	0	0	0	0	0	0	0	0	0
375	5612	1	0	0	2	0	0	0	0	0	0	0	0
365	5338	1	0	0	1	0	0	0	0	0	0	0	0
355	5065	6	3	1	2	6	5	2	0	0	0	0	0
346	4819	4	0	0	0	3	4	0	0	0	0	0	0
340	4655	3	0	0	0	2	2	0	0	0	0	0	0
335	4518	5	2	0	0	0	0	0	0	0	0	0	0
330	4381	0	0	0	4	0	0	0	1	0	0	0	0

Depth (cm)	Age (Cal. yr. BP)	*S. fusiformis*	*E. hallandense*	*S. groenlandica*	*F. laevigata*	*C. teretis*	*C. laevigata*	*T. trihedra*	*D. Trondheimensis*	*Globobulimina Sp.*	*D. drammenensis*	*L. clavata*	*L. linearis*
325	4245	1	0	0	0	0	0	0	0	0	0	0	0
320	4108	0	1	0	1	0	0	0	0	0	0	0	0
315	3971	4	0	0	0	0	0	0	0	2	0	0	0
310	3835	1	1	0	1	1	0	0	0	0	0	0	0
300	3561	2	0	0	0	0	0	0	0	0	0	0	0
296	3452	1	0	0	0	4	0	0	0	0	0	0	0
285	3151	2	1	0	0	0	1	1	0	2	0	0	0
280	3015	2	2	0	2	1	2	2	0	1	0	0	0
275	2878	1	0	0	1	0	0	0	0	0	0	0	0
265	2605	2	0	0	0	0	0	0	0	0	0	0	0
255	2331	1	0	0	0	0	1	1	0	0	0	0	0
250	2195	2	0	0	0	0	0	0	0	0	0	0	0
245	2058	1	1	0	0	0	0	0	0	0	0	0	0
240	1921	1	2	0	0	0	0	0	0	0	0	0	0
235	1784	0	2	0	0	0	0	0	0	0	0	0	0
230	1648	1	1	0	0	0	0	0	0	0	0	0	0
225	1511	4	1	0	0	0	0	0	0	0	0	0	0
215	1238	3	1	0	0	0	0	0	0	0	0	0	0
210	1101	1	2	0	0	0	0	0	0	0	0	0	0
205	964	2	0	0	0	0	0	0	0	0	0	0	0
200	828	1	0	0	0	0	0	0	0	0	0	0	0
195	691	6	1	0	0	0	0	0	0	0	0	0	0
185	650	5	0	0	0	0	0	0	0	0	1	0	0
175	609	2	2	0	0	0	0	0	0	0	1	0	0
165	569	3	1	0	0	0	0	0	0	0	0	0	0
155	528	6	6	0	0	0	2	3	0	0	1	0	0

Depth (cm)	Age (Cal. yr. BP)	*S. fusiformis*	*E. hallandense*	*S. groenlandica*	*F. laevigata*	*C. teretis*	*C. laevigata*	*T. trihedra*	*D. Trondheimensis*	*Globobulimina Sp.*	*D. drammenensis*	*L. clavata*	*L. linearis*
145	487	1	0	0	0	0	0	0	0	0	0	0	0
140	467	2	1	0	0	0	0	0	0	0	0	0	1
135	446	0	0	0	0	0	0	0	0	0	0	0	0
130	426	0	0	0	0	0	0	0	0	0	0	0	0
125	406	0	0	0	0	0	0	0	0	0	0	0	0
120	385	0	1	0	0	0	0	0	0	0	0	0	0
115	365	0	0	0	1	0	0	0	0	0	0	0	0
110	345	0	0	0	0	0	0	0	0	0	0	0	0
106	328	0	0	0	0	0	0	0	0	0	0	0	0
100	304	0	0	0	0	0	0	0	0	0	0	0	0
94	279	1	0	0	0	0	0	1	0	0	0	0	0
90	263	0	1	0	0	0	0	0	0	0	0	0	0
85	243	3	0	0	0	0	0	0	0	0	0	0	0
80	222	0	0	0	0	0	0	0	0	0	0	0	0
75	202	0	0	0	0	0	0	0	0	0	0	0	0
70	182	1	0	0	0	0	0	0	0	0	0	0	0
65	161	1	0	0	0	0	0	0	0	0	0	0	0
60	141	0	0	0	0	0	0	0	0	0	0	0	0
55	120	2	0	0	0	0	0	0	0	0	0	0	0
50	100	0	0	0	0	0	1	0	0	0	0	0	0
45	80	0	0	0	0	0	0	0	0	0	0	0	0
40	59	0	0	0	0	0	0	0	0	0	0	0	0
35	39	2	1	0	0	0	1	0	1	0	0	0	0
25	-2	2	2	0	0	0	0	0	1	0	0	0	0
20	-22	2	0	0	0	0	0	0	0	0	0	1	0
15	-43	1	0	0	1	0	0	0	0	0	0	0	0

Depth (cm)	Age (Cal. yr. BP)	*S. fusiformis*	*E. hallandense*	*S. groenlandica*	*F. laevigata*	*C. teretis*	*C. laevigata*	*T. trihedra*	*D. Trondheimensis*	*Globobulimina Sp.*	*D. drammenensis*	*L. clavata*	*L. linearis*
10	-63	0	1	0	0	0	0	0	0	0	0	0	0
5	-63	0	0	0	0	0	0	0	0	0	0	0	0
0	-63	0	0	0	1	0	0	0	0	0	0	0	0

Appendix 4 – Species abundance

This appendix contains the relative abundance of each of the 10 most common species at sampling depths within core HH13-012GC-TUNU, and their average abundance within each of the assemblage zones. Samples containing less than 100 specimens are left out.

Depth (cm)	Age (Cal yr. BP)	% *C. reniforme*	% *E. excavatum*	% *I. Helenae*	% *I. norcrossi*	% *S. loeblichi*	% *Q. stalkeri*	% *A. gallowayi*	% *C. lobatulus*	% *T. tricarinata*	% *H. orbiculare*
454	7771	60,06	5,52	28,90	2,27	1,62	0,32	0,00	1,30	0,00	0,00
444	7498	65,91	3,03	21,21	0,00	1,52	1,52	0,00	0,00	0,00	0,00
435	7252	52,36	21,62	23,31	1,01	1,69	0,00	0,00	0,00	0,00	0,00
425	6978	62,21	8,14	23,13	0,33	2,61	0,65	0,00	0,00	0,33	0,00
415	6705	53,11	6,89	34,43	0,00	2,30	0,00	0,00	0,00	0,00	0,00
405	6432	53,21	8,33	33,33	0,00	1,28	0,00	0,00	0,64	0,96	0,00
395	6158	46,93	2,59	47,25	0,00	0,65	0,32	0,00	0,65	0,32	0,00
385	5885	61,24	7,82	12,38	0,00	0,98	0,00	1,30	14,33	0,00	0,00
375	5612	54,07	7,17	20,85	0,00	1,95	0,00	0,65	12,38	0,00	0,00
365	5338	37,25	3,92	42,81	1,31	0,98	0,00	1,63	4,25	0,33	4,58
355	5065	47,04	18,03	5,26	0,00	4,28	3,62	2,30	0,00	0,00	2,63
346	4819	55,22	5,97	14,93	0,00	0,75	10,82	2,24	0,00	0,00	1,12
340	4655	52,99	10,68	11,11	0,00	0,85	5,98	11,54	0,00	0,85	2,99
335	4518	48,57	11,43	7,35	0,00	0,41	2,45	11,84	0,00	8,98	4,49
330	4381	52,40	2,40	25,96	1,44	4,81	1,92	3,37	0,00	5,29	0,00
325	4245	52,08	6,25	17,19	0,00	1,56	0,52	18,75	0,00	0,52	2,60
320	4108	54,82	17,28	15,61	0,33	0,66	0,66	7,97	0,00	1,99	0,00
315	3971	45,85	1,66	6,98	0,33	1,33	1,33	35,88	0,00	4,65	0,00
310	3835	49,25	16,22	10,21	1,20	0,90	1,80	18,32	0,00	0,90	0,00
300	3561	51,13	34,41	0,96	0,96	0,96	0,64	9,65	0,00	0,64	0,00
296	3452	49,01	2,32	4,30	0,33	0,99	2,65	38,08	0,00	0,66	0,00

Depth (cm)	Age (Cal yr. BP)	*% C. reniforme*	*% E. excavatum*	*% I. Helenae*	*% I. norcrossi*	*% S. loeblichi*	*% Q. stalkeri*	*% A. gallowayi*	*% C. lobatulus*	*% T. tricarinata*	*% H. orbiculare*
285	3151	53,19	2,13	8,09	0,85	0,85	1,70	26,38	0,43	2,13	0,85
280	3015	52,48	2,48	5,37	0,41	1,24	2,48	26,45	0,00	2,48	1,24
275	2878	58,64	1,82	6,36	0,00	0,91	0,91	28,18	0,00	1,82	0,45
265	2605	73,03	1,32	3,62	0,33	2,30	1,32	16,78	0,00	0,33	0,33
255	2331	60,26	2,28	5,21	0,00	2,28	2,28	25,73	0,00	2,28	0,33
250	2195	41,54	26,54	2,69	0,38	1,54	4,62	20,00	0,00	1,92	0,00
245	2058	46,33	2,82	7,34	0,00	1,13	9,04	30,51	0,00	1,69	0,00
240	1921	37,28	37,57	2,37	0,30	0,59	2,96	15,38	0,30	1,78	0,59
235	1784	46,23	3,02	2,51	0,00	0,50	3,02	43,22	0,00	0,50	0,00
230	1648	51,28	29,63	3,42	1,42	0,57	4,84	5,98	0,00	1,71	0,57
225	1511	56,77	1,31	2,62	0,00	0,44	3,06	32,75	0,00	0,87	0,00
215	1238	34,32	18,81	0,00	0,33	0,66	1,98	40,59	0,00	1,32	0,66
210	1101	34,66	42,05	2,84	0,57	1,70	1,14	11,93	0,00	1,70	1,70
200	828	70,97	18,55	1,61	0,40	0,81	1,21	4,84	0,00	1,21	0,00
195	691	50,33	9,21	6,58	1,64	0,66	5,59	22,37	0,00	0,99	0,00
185	650	52,74	0,08	7,53	2,05	0,00	0,00	17,81	0,00	7,53	0,00
175	609	59,21	14,47	6,91	0,33	1,32	0,33	14,14	0,00	1,64	0,00
165	569	25,24	43,13	0,32	0,00	0,32	0,96	27,16	0,00	1,28	0,32
155	528	48,54	28,16	1,29	0,32	1,29	1,62	9,06	0,00	3,88	0,00
145	487	57,87	26,39	0,00	0,00	0,46	0,93	12,04	0,00	1,39	0,00
140	467	45,53	36,18	0,41	0,41	0,41	0,00	14,23	0,00	1,22	0,00
125	406	32,38	47,62	0,00	0,95	0,00	2,86	14,29	0,00	0,95	0,00
120	385	33,58	44,53	0,00	1,46	2,92	5,11	10,22	0,00	1,46	0,00
94	279	51,49	29,10	0,75	0,75	0,00	8,96	5,97	0,00	1,49	0,00
90	263	57,74	25,00	0,00	0,60	1,19	5,36	8,33	0,00	1,19	0,00
85	243	52,54	28,99	3,99	2,17	1,09	5,07	4,71	0,00	0,00	0,00
70	182	32,86	46,43	3,57	0,00	0,71	4,29	10,71	0,00	0,71	0,00

Depth (cm)	Age (Cal yr. BP)	% *C. reniforme*	% *E. excavatum*	% *I. Helenae*	% *I. norcrossi*	% *S. loeblichi*	% *Q. stalkeri*	% *A. gallowayi*	% *C. lobatulus*	% *T. tricarinata*	% *H. orbiculare*
65	161	52,49	32,13	0,00	0,45	0,45	7,69	4,98	0,00	0,90	0,00
50	100	62,20	20,47	0,00	1,57	1,57	7,09	4,72	0,00	1,57	0,00
40	59	64,66	19,55	0,75	1,50	0,75	9,02	1,50	0,00	2,26	0,00
35	39	51,27	28,34	1,59	0,64	0,32	4,46	11,15	0,00	0,64	0,00
25	-2	37,06	37,56	1,52	1,52	0,00	10,66	7,61	0,00	1,52	0,00
20	-22	42,28	34,90	1,34	0,67	1,34	5,37	8,72	0,00	3,36	0,00
15	-43	60,83	15,00	0,83	0,83	0,00	8,33	10,83	0,00	1,67	0,00
10	-63	62,75	22,22	0,00	0,00	0,65	2,61	10,46	0,00	0,65	0,00
0	-63	41,84	34,69	0,00	1,02	0,00	8,16	13,27	0,00	0,00	0,00
Depth	**Assemblage zone:**	**Average *C. reniforme***	**Average *E. excavatum***	**Average *I. helenae***	**Average *I. norcrossi***	**Average *S. loeblichi***	**Average *Q. stalkeri***	**Average *A. gallowayi***	**Average *C. lobatulus***	**Average *T. tricarinata***	**Average *H. orbiculare***
454-360	**AZ3**	54,64	7,50	28,76	0,49	1,56	0,28	0,36	3,35	0,19	0,46
360-180	**AZ2**	51,05	12,08	6,96	0,49	1,25	2,91	19,59	0,03	2,03	0,76
180 - 0	**AZ1**	48,62	30,74	1,16	0,76	0,74	4,94	10,21	0,00	1,39	0,02

Appendix 5 – Foraminiferal flux

This appendix contains the total foraminiferal flux, and the foraminiferal concentration at all sampled depths within core HH13-012GC-TUNU, in addition to average foraminiferal flux within each of the assemblage zones.

Depth (cm)	Age (Cal yr. BP)	Sedimentation rate	Total number of foraminifera	Foraminiferal concentration	Total foraminiferal flux
454	7771	36	308	18,7	1208,6
444	7498	36	132	4,8	311,9
435	7252	36	296	8,2	528,4
425	6978	36	307	32,9	2132,5
415	6705	36	305	40,2	2604,0
405	6432	36	312	68,5	4435,6
395	6158	36	309	51,8	3358,2
385	5885	36	307	9,7	625,5
375	5612	36	307	29,5	1908,6
365	5338	36	306	74,1	4802,5
355	5065	36	304	10,9	707,0
346	4819	36	268	9,0	581,2
340	4655	36	234	7,0	451,0
335	4518	36	245	6,8	440,8
330	4381	36	208	6,1	398,3
325	4245	36	192	5,9	379,5
320	4108	36	301	11,5	745,6
315	3971	36	301	17,9	1161,5
310	3835	36	333	13,1	849,0
300	3561	36	311	11,6	750,2
296	3452	36	302	14,9	966,7
285	3151	36	235	5,2	335,0
280	3015	36	242	6,2	399,0
275	2878	36	220	5,5	359,0
265	2605	36	304	9,2	594,6
255	2331	36	307	11,3	735,2
250	2195	36	260	5,4	349,1
245	2058	36	177	4,4	284,3
240	1921	36	338	7,8	506,4
235	1784	36	199	5,3	343,3
230	1648	36	351	11,6	753,4
225	1511	36	229	7,8	503,7
215	1238	36	303	10,6	685,8
210	1101	36	176	5,5	353,3
205	964	36	47	1,3	84,5
200	828	36	248	6,2	399,7

Depth (cm)	Age (Cal yr. BP)	Sedimentation rate	Total number of foraminifera	Foraminiferal concentration	Total foraminiferal flux
195	691	36	304	6,1	395,6
185	650	279	146	3,8	1892,6
175	609	279	304	7,0	3505,2
165	569	279	313	8,8	4429,8
155	528	279	309	9,5	4791,9
145	487	279	216	6,0	3015,7
140	467	279	246	6,7	3385,6
135	446	279	72	2,2	1096,7
130	426	279	85	2,5	1252,2
125	406	279	105	3,4	1687,4
120	385	279	137	5,1	2585,5
115	365	279	51	1,3	669,1
110	345	279	52	1,8	924,7
106	328	279	55	2,1	1045,9
100	304	279	50	1,5	744,0
94	279	279	134	2,4	1227,3
90	263	279	168	4,2	2126,3
85	243	279	276	6,3	3188,6
80	222	279	86	2,0	1000,2
75	202	279	82	2,0	990,6
70	182	279	140	3,1	1546,6
65	161	279	221	7,3	3643,7
60	141	279	85	2,6	1288,5
55	120	279	87	3,1	1541,7
50	100	279	127	4,0	1995,6
45	80	279	85	2,4	1207,6
40	59	279	133	2,7	1361,4
35	39	279	314	7,6	3805,9
25	-2	279	197	5,0	2535,5
20	-22	279	149	4,8	2393,7
15	-43	279	120	2,8	1414,3
10	-63	279	153	4,1	2040,3
5	-63	279	70	1,9	938,7
0	-63	279	98	1,9	949,6

Assemblage zone	Depth (cm)	Age (cal. yr. BP)	Average foraminiferal flux
AZ 3	454 - 360	7771 - 5221	2191,6
AZ 2	360 - 180	5221 - 630	585,9
AZ 1	180 - 0	630 - -63	2010,3